LBL-10005

Lawrence Berkeley Laboratory
UNIVERSITY OF CALIFORNIA

Materials & Molecular
Research Division

KINETICS OF CLUSTERING REACTIONS

E. S. Pundarika
(Ph.D. thesis)

August 1979

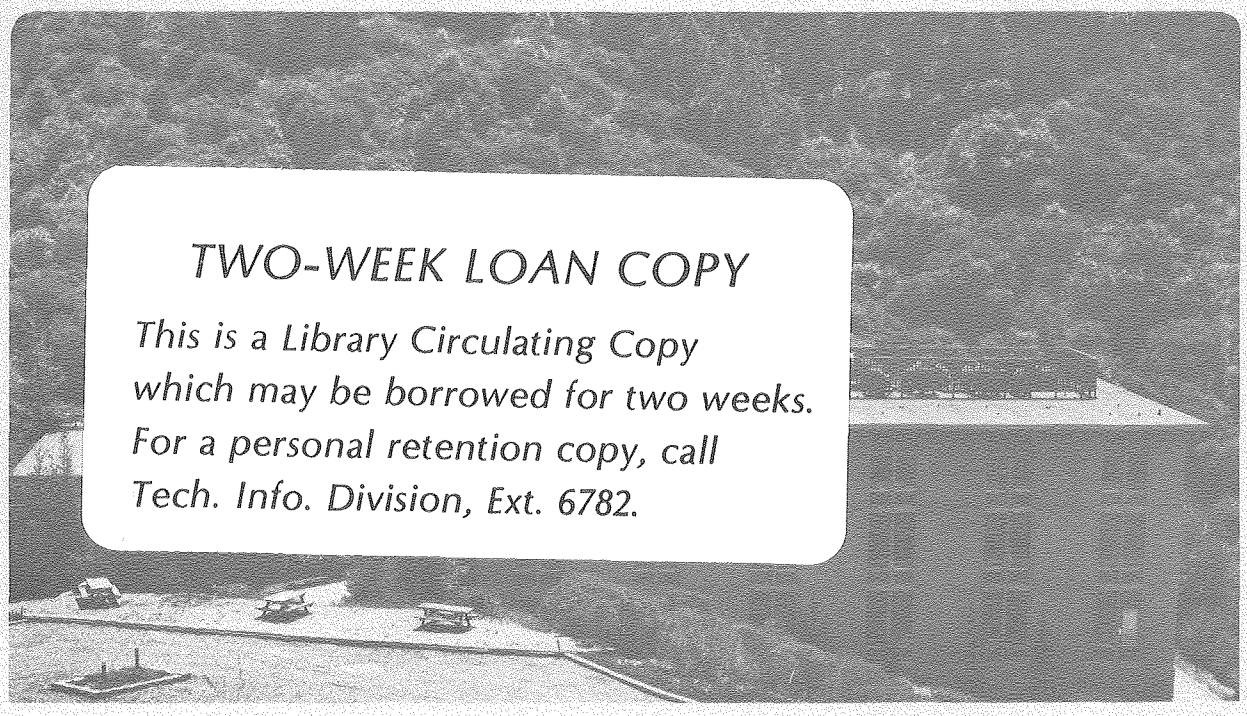

Prepared for the U.S. Department of Energy under Contract W-7405-ENG-48

DISCLAIMER

KINETICS OF CLUSTERING REACTIONS

E.S.Pundarika

Department of Materials Science and Mineral Engineering
and Materials and Molecular Research Division
Lawrence Berkeley Laboratory
University of California
Berkeley, California 94720

ABSTRACT

The dynamics of precipitation and coarsening reactions in a binary Ising lattice are studied using a simulation technique. The initial random configuration represents equilibration at a very high temperature. Following a quench to the reaction temperature below the miscibility gap, the decomposition proceeds by atomic interchanges of matrix and impurity atoms. The probability of such interchanges depends on the reaction temperature as also the local environ of the particular atom pair that is interchanging. Both the excess energy $\langle \epsilon - \epsilon_\infty \rangle$ and the average cluster size $\langle n \rangle$ are found to follow simple power law relations with time, $\langle \epsilon - \epsilon_\infty \rangle = t^{-b}$ and $\langle n \rangle = t^{a}$. For the square lattice, Binder's cluster diffusion and coagulation mechan-

ism is seen to dominate the coarseninig reactions at early times, in agreement with the studies of Lebowitz et al. The early time exponent (a) correspondingly has a value close to 0.2. However, at later times, the mechanism changes over to a Lifshitz and Slozov atom by atom transfer mechanism, as the cluster size becomes larger. The nature of this changeover is seen to depend primarily on the temperature; the two regions overlap at higher temperatures and are separated by a long incubation period at lower temperatures. The different regions are closely associated with the relative bond type populations which reach asymptotic values as Lifshitz Slozov coarsening stage begins.

KINETICS OF CLUSTERING REACTIONS

E. S. PUNDARIKA

INTRODUCTION

A variety of important metallurgical phenomena are controlled by the nature and kinetics of precipitation reactions and precipitate coarsening processes. The relevant phenomena include precipitation hardening and aging processes in alloys and void formation and swelling in irradiated materials. Coarsening is driven by the eventual decrease of surface free energy and the final stage of coarsening would be a single precipitate with an interphase of minimum possible energy. Interestingly, this stage is never reached in times that concern practical materials, so usually the kinetics rather than the equilibrium are of more importance. Also, the most striking influence on properties is often sees during the first stages of precipitation unless the precipitates contain only a few atoms or unit cells and the precipitate distribution is far from equilibrium, necessitating a thorough understanding of the initial stages of precipitation and coarsening reactions.

Theoretical analysis[1-6] have given useful insights into these processes. These theories are based on free energy vs. composition plots and are basically continuum in nature and assume quasi-equilibrium conditions.

The coarsening process is simplest in its late stages, when the particles are large and essentially immobile and classic "Ostwald ripening" occurs through single atom diffusion between clusters. The net mass transport is to the larger particles so as to decrease the total surface energy of the system. The rate of mass transport may be controlled either by surface reactions (dissolution or adsorption) or by diffusion in the bulk. The latter case has been analyzed in detail by Lifshitz and Slozov[3] and will be denoted "LS coarsening" in the following.

The Lifshitz-Slozov analysis predicts that both the excess energy $\langle \epsilon - \epsilon_\infty \rangle$ where ϵ_∞ is the equilibrium value of the energy, and the average cluster size $\langle n \rangle$ will obey simple power laws in time:

$$\langle n \rangle = A\, t^{a} \qquad \text{I.1}$$

$$\langle \epsilon - \epsilon_{\infty} \rangle = B\, t^{-b} \qquad \text{I.2}$$

The analysis also provides a scaling law which establishes the distribution of cluster sizes about the expected value $\langle n \rangle$. It hence predicts a very simple coarsening behaviour which can be easily understood.

There are, however, assumptions inherent to the LS analysis which confine it to the later stages of coarsening. These include the neglect of particle geometry and the assumption of particle immobility. While recent work seems to establish that the LS assumption of spherical geometry is not critical to their result[15], the assumption of a size-independent surface tension is critical and, as we shall discuss further below, is not likely to hold for small precipitates in crystalline solids. The assumption of particle immobility is also invalid when the particle size is small. Small clusters of atoms can diffuse at an appreciable rate while remaining intact and may contribute to coarsening by coagulation directly with one another.

The process of coarsening through the diffusion and direct coagulation of clusters was studied in detail by Binder[6]. While Binder analysis is not free of assumptions, these do not explicitly constrain the sizes, shapes, or distributions of the clusters. However since the cluster diffusivity decreases with size as $n^{-1-1.5}$, Binder process should become less dominant at later times. Binder also obtains simple power laws for the time dependence of the excess energy and the average cluster size. These are

$$\langle n \rangle = Ct^{a} \qquad \text{I.3}$$

$$\langle \epsilon - \epsilon_{\infty} \rangle = Dt^{-b} \qquad \text{I.4}$$

where $a = 0.4\text{-}0.5$ and $b = 0.2\text{-}0.25$, for the two-dimesnional case.

While the Binder and Lifshitz-Slozov analyses span a good part of the coarsening behaviour of real solids, the restrictions imposed by the assumptions underlying these theoretical models are not entirely clear, nor are their limits of applicability obvious. With the development of

computer techniques it has become possible to conduct direct computer simulation studies of coarsening in idealized systems, such as the Ising lattice in two or three dimensions[8-13]. The computer studies have the disadvantage that they treat model rather than real systems, but have the compensating advantage that they represent clear-cut "experiments" which may be used to test the applicability of the theories and to investigate interesting aspects of the coarsening process in detail.

Computer simulation studies have shown the dominance of the cluster coagulation mechanism in the early stages of coarsening[10] and have revealed slope changes in the plots of excess energy against time which indicate the expected shift to LS coarsening behaviour in the later stages. These earlier researches are extended in the computer simulation studies reported below, which focus on the simple case of a two-dimensional Ising lattice and attempt a reasonably comprehensive exploration of coarsening behaviour as a func-

tion of time, temperature and composition.

The binary Ising lattice was the most obvious choice for out model, since its equilibrium properties (in the absence of an external field) have been very well characterized. We began this research project with a view to characterizing the kinetics of precipitation and coarsening reactions in our model lattice. The results of the above mentioned theories should certainly be applicable to our simple model since the requirements of these theories are more than satisfied here. Hence the results obtained in our simulations can be used as a straight forward test of the applicability of these theories.

The model used for the computer simulation will be described in Chapter 2. A simple exchange model where atoms of two types, initially distributed randomly on a lattice, redistribute themselves in discrete steps of atomic interchanges forms the basis of the simulation. The probabilities of atomic interchanges are controlled by global variables

(such as temperature) and more importantly by the local environ of the atom pair. The local environ is limited in our studies to the first nearest neighbours of the atoms involved, but can be easily extended to include second or third nearest neighbours as well. Whether the resulting redistribution of atoms leads to clustering or ordering depends upon whether the interaction energy of the atoms of two types is positive or negative.

Study of this model and its characterization in terms of its coarsening behaviour forms the subject matter of this research project, detailed in Chapter 3.

In Chapter 4 the computer simulation technique, whereby the process described by our physical model is put into action is described. Although the process as described in Chapter 2 can be directly translated into a code, this is not a good way of doing it because of the enormous amount of time needed for the simulation run. A deeper look into our own physical model shows shortcuts which can be used

beneficially to increase the program speed. Further the idiosyncracies of the computer must also be considered and constructively used in this respect.

The results of our simulation work and discussions form the subject matter of Chapter 5. The first section describes the basic four stage reaction that the decomposition follows. In the initial relaxation stage a large amount of lattice energy is decreased resulting from the formation of small clusters of upto 10 atoms. In the second stage there is a diffusive movement of these small clusters, leading to their eventual coagulation and coarsening. Such diffusive movement of clusters becomes less important as their size increases. This marks the beginning of stage 3. In this stage the surface profile of the clusters reaches an equilibrium. In stage 4 or steady state the coarsening reaction is mainly by atom by atom transfer mechanism or Lifshitz and Slozov mechanism. Sections 2, 3 and 4 discuss the effects of temperature, lattice type and composition on this basic

four stage coarsening reaction. The characterization of cluster properties, including their distributions is dealt with in section 5.

Finally in Chapter 6 the results are summarized and conclusions are drawn.

MODEL

The simplest realistic case of a binary Ising lattice with nearest neighbour interactions only in zero magnetic field is chosen. The two spins are taken to represent the two types of atoms A and B. Under this assumption the thermodynamics of the lattice are known to be governed by the lattice type and by the interaction parameter

$$J = E_{AB} - 1/2(E_{AA} - E_{BB}) \qquad \text{II.1}$$

where E_{ij} is the energy of a bond between atoms of types i and j. The total number of atom pairs in the lattice is

$$N = 1/2 N_o Z \qquad \text{II.2}$$

where Z is the number of nearest neighbours of an atom. If N_{AB} is the number of AB atom pairs, then the relative energy per bond (atom pair) is in units of J,

$$\epsilon = \frac{N_{AB}}{N} \qquad \text{II.3}$$

For any given distribution of A and B atoms (spins), the energy of the lattice is given by :

$$E = -J \sum_{i,j} n_i n_j \qquad \text{II.4}$$

in terms of η_i and η_j, the occupation numbers (+1 for A and -1 for B) and the sum is taken over the nearest neighbour atoms only. This type of interaction leads at low temperatures either to a phase segregation when J>0 (corresponding to an excess attraction between atoms of the same type) or to ordering when J<0 (corresponding to an excess attraction between atoms of the opposite type).

The equilibrium properties for this model have been very well characterized. In fact, exact analytical results for partition function, critical temperature, phase diagram etc., are available for certain two dimensional lattices. Numerical methods have been developed for cases (such as 3d) which are not yet amenable to analytical calculations. All these have been extensively reviewed[8].

For the case of square lattice, the critical temperature is given by :

$$kT_c = 2.414J \qquad \text{II.5}$$

and the phase diagram is given by :

$$C(\text{phase}) = \frac{1}{2}\left\{\left[1-\frac{16x^4}{(1-x^2)^4}\right]^{1/8}+1\right\} \qquad \text{II.6}$$

where $x = \exp(-2J/kT)$.

Similarly for the case of the two dimensional hexagonal lattice (triangular lattice) we have :

$$kT_c = 3.2435J \qquad \text{II.6}$$

$$C(\text{phase}) = \frac{1}{2}\left\{\left[1-\frac{16x^6}{(1+3x^2)(1-x^2)^3}\right]^{1/8}+1\right\} \qquad \text{II.7}$$

It is important to see that the square lattice is symmetrical with respect to J or -J. That is it has the same phase diagram for the ordering and clustering cases. For the case of the hexagonal lattice $T_c = 0$ for $J<0$. That is no order-disorder transformation exists for this case. However, it shows a clustering behaviour with the above phase diagram and T_c for $J>0$.

Having based ourselves on this model with well characterized equilibrium properties, we can study the kinetics of clustering or ordering reactions by developing the dynamic

aspects of the model. In this research project, the basic diffusion step is taken to be interchange of nearest neighbour atoms. Further this interchange is assigned a probability P based on the temperature T and the energy change ΔE resulting from such an interchange. We are now ready to study the kinetics of the clustering or ordering reactions. In real systems such reactions are studied by quenching specimens equilibrated at high temperature to the reaction temperature, and following the changes in the specimen. In our model also a similar study can be done.

The A and B atoms are initially distributed randomly over the lattice sites. This random distribution in our model represents equilibration at/above a very high temperature where the configurational entropy is dominant. (For an infinite lattice and for an infinite lattice only, this temperature is infinite). When the lattice is quenched from this high temperature to some low temperature the atoms will assume a configuration of lower energy as dictated by the

thermodynamics. The reaction will be either a clustering or an ordering reaction depending on whether the energy of the A-B interaction is such that the atoms have an energetic preference for the neighbours of like kind ($J>0$) or for neighbours of unlike kind($J<0$). Jump probabilities are assigned to different atom exchanges based on the reaction temperature and the energy change ΔE of the system. The reaction is then allowed to proceed (jump by jump) as per the probabilities, and the properties of the system are followed kinetically.

The amenability of our model to computer simulation is now very clear from the description of the dynamics of the model above. In fact, the steps above, followed as such, can form the basis of a Monte Carlo type simulation. The details of the computer simulation technique will be described in Chapter 4.

Exchange Probability:

Consider an exchange of atoms at lattice positions j and 1 (j and 1 are nearest neighbours of each other). The initial energy before exchange is given by

$$E_{initial} = -\frac{1}{2}J(\sum_i \eta_i \eta_j + \sum_k \eta_k \eta_1 + X) \qquad \text{II.8}$$

where η_i = depending on whether there is an A or a B atom at that site, i and k are the sums over the nearest neighbour sites of j and 1, and X represents similar sums over the other lattice sites. The final energy after exchange is similarly

$$E_{final} = -\frac{1}{2}J\left[\sum_i \eta_i \eta_1 + \sum_k \eta_k \eta_j + X\right] \qquad \text{II.9}$$

The energy change

$$\begin{aligned} \Delta E_{j1} &= E_{final} - E_{initial} \\ &= -\frac{1}{2}J\left[\sum_i \eta_i \eta_1 + \sum_k \eta_k \eta_j\right] + \frac{1}{2}J\left[\sum_i \eta_i \eta_j + \sum_k \eta_k \eta_1\right] \qquad \text{II.10} \\ &= -\frac{1}{2}J\left[\sum_i \eta_i (\eta_1 - \eta_j) + \sum_k \eta_k (\eta_j - \eta_1)\right] \end{aligned}$$

That is

$$\Delta E_{j1} = -\frac{1}{2}J(\eta_1 - \eta_j)\left[\sum_i \eta_i - \sum_k \eta_k\right] \qquad \text{II.11}$$

It is clearly seen from this formula that the energy change for the reverse jump $\Delta E_{1j} = -\Delta E_{j1}$.

The exchange probability should depend on this energy change ΔE_{j1}, as also on the temperature T. Many different expressions have been used for the probability P_{j1}. In their original paper Metropolis et al.[9] used

$$\begin{aligned} P_{j1} &= 1 && ,\Delta E_{j1} \leq 0 \\ P_{j1} &= \exp(-\Delta E_{j1}/kT) && ,\Delta E_{j1} > 0 \end{aligned} \qquad \text{II.12}$$

In our model we use

$$P_{j1} = \frac{\exp(-\Delta E_{j1}/kT)}{\left[1 + \exp(-\Delta E_{j1}/kT)\right]} \qquad \text{II.13}$$

for both $\Delta E_{j1} \leq 0$ and $\Delta E_{j1} > 0$. A recent study has shown that our choice yields greater stability and faster convergence[10].

Using the relationship between J and T_c (for example $J = 0.8814kT_c$ for square lattice), we can eliminate J from ΔE_{j1}. Further the temperature T can be expressed in the dimensionless units of T/T_c. The jump probability then takes on the simple form :

$$P_{jl} = \frac{e^{-\beta\Delta n_{jl}}}{1 + e^{-\beta\Delta n_{jl}}} \qquad \text{II.14}$$

where,

$$\begin{aligned} \beta &= \frac{J}{kT_{real}} \\ &= 0.8814\left(\frac{T_c}{T}\right) \\ &= \frac{0.8814}{T_{dimensionless}} \\ &= \frac{0.8814}{T} \end{aligned} \qquad \text{II.15}$$

$$\Delta n_{jl} = \Delta\frac{E_{jl}}{J}$$

$$= -\frac{1}{2}(\eta_l - \eta_j)\left[\sum_i \eta_i - \sum_k \eta_k\right]$$

P_{jl} represents the probability of exchange per unit time, and hence is directly related to the rate of exchange. In other words, these probabilities can be used to keep track of the time of the reaction. This will be discussed in Chapter 4. The equations governing the kinetics of evolution of the binary Ising lattice may be cast into a form which is particularly well suited for computer simulation studies. Chapter 4 will discuss this important topic of correlation of the simulation with the model presented here. The formulations presented follow that previously used in

the kinetic analysis of thermally-activated deformation processes[19] and martensitic transformations[20,21] and is drawn largely from Feller[22].

PURPOSE AND SCOPE OF THE PRESENT INVESTIGATION

The theoretical treatments of coarsening generally consider steady state, or very late stages of coarsening, where the coarsening rate is surface reaction controlled or diffusion controlled. The latter has been analyzed in detail by Lifshitz and Slozov and is conveniently called Lifshitz-Slozov or LS mechanism. Coarsening here occurs by mass transport by single atom diffusion between clusters, driven by the eventual decrease in total surface energy.

Recently Binder has analyzed the coarsening of clusters by Binder's mechanism : diffusion and coagulation of clusters. Here atoms of clusters move around in the cluster itself either through the cluster or through the matrix, leading to a random walk and eventual coagulation of clusters. Depending on whether the cluster diffusion is by movements of atoms through the body of the cluster or

through its volume, the diffusivity of a cluster of size n, varies as n^{-1} or $n^{-1.5}$. Thus the Binder's mechanism should become less important as the average cluster size <n> increases.

The generalized features of the clusters which are of importance in initial stages is not considered in these theories. For example the LS analysis assumes that the interfacial energy is independent of the cluster size. This assumption is questionable at small cluster sizes, and the simulation results indicate that the cluster surface energy levels off after some cluster size. The LS theory also assumes spherical particles (isotopic surface tensions), but this assumption is not critical, as long as particles have their equilibrium shapes[11].

Both the Binder and the LS mechanisms predict simple power laws for the variation of excess energy $\langle \phi - \phi_\infty \rangle$ and the average cluster size as follows:

$$\langle n \rangle = t^{a} \qquad \text{III.1}$$

$$\langle n \rangle = t^{-b} \qquad \text{III.2}$$

where:

LS — a = 0.66; b = 0.33

Binder — a = 0.4 - 0.5; b = 0.2 - 0.25

It is thus possible to follow these mechanisms by following the slopes of $\langle n \rangle$ vs t or $\langle \epsilon - \epsilon_{\infty} \rangle$ vs t curves. In addition, in our simulation approach, we have the further advantage of being able to actually trace through the atomic steps and be able to interpret the former results objectively. This advantage is especially significant at the small cluster sizes, since then the assumptions of neither theory (especially regarding the geometry of clusters) are satisfied.

Previous studies of this type have shown that Binder's mechanism dominates at the early stages of the process for the 2-d case[7]. It has also been pointed out that for the 3-d case the LS mechanism should prevail at earlier times than 2-d[6]. A slope change to a higher value corresponding

to the LS mechanism at late stages in the $<\epsilon-\epsilon_\infty>$ vs t plots also has been reported[7]. However, percolation effects hinder a meaningful study of the cluster sizes in 3-d.

This investigation was begun with the objective of studying and characterizing the kinetics of clustering reactions in a binary Ising lattice. The method of approach used is the direct computer simulation of the atomic diffusion process. The following topics are covered:

(1) Square lattice

(a) the basic coarsening reaction

(b) effect of process parameters such as T, composition on (a)

(2) Hexagonal lattice

Simulation and comparison with (1)

The phase diagram of the two-dimensional square Ising lattice is plotted in Figure 1. The figure also contains a

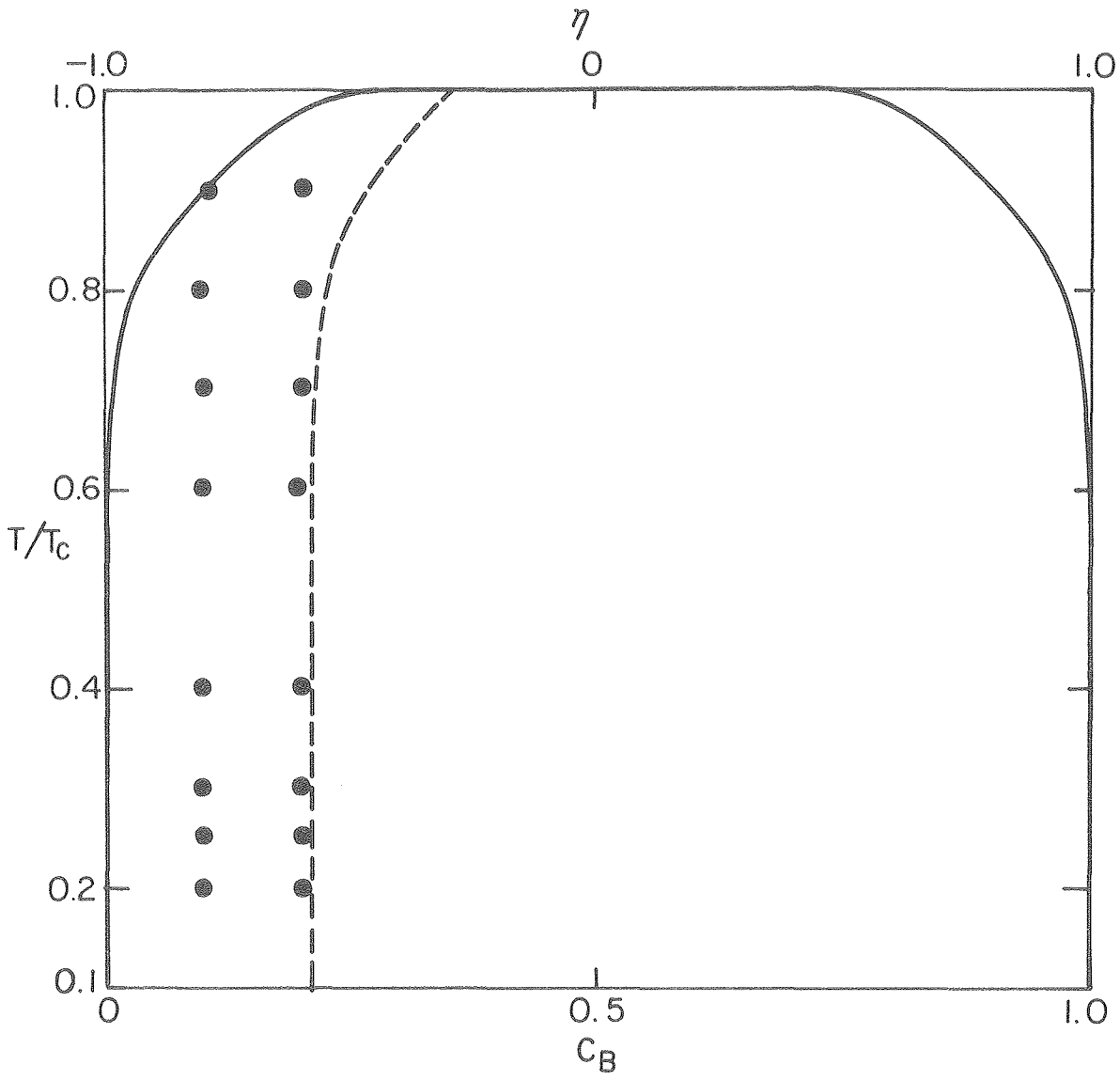

Fig. 1. Phase diagram of the binary Ising square lattice, indicating the points of simulation reported here. The dotted line shows the limit of metastability, assuming a free energy density of the form $f(C_{cr}) = A(C-C_{cr})^2+B(C-C_{cr})^4+f(C_{cr})$ where C_{cr} is the concentration at the phase boundary.

plot of spinodal limits, or inflection points of the free energy of a hypothetical lattice of homogeneous composition, computed under the approximation that the free energy within the miscibility gap is given by the fourth order polynomial[15]:

$$F(c) = F(c_e^*)+A(c-c_e^*)^2+B(c-c_e^*)^4 \qquad \text{III.3}$$

This polynomial approxiamation is known to be inaccurate at bery low temperature (the spinodal curve must join the equilibrium curve at t=0), but gives a reasonable approximation over much of the temperature range.

The qualitative behaviour of the system can be predicted from the equilibrium phase diagram. If the binary solution is equilibrated at very high temperature, the A and B atoms will be randomly distributed over its lattice sites. If the system is then quenched to a temperature within the miscibility gap, the lattice will begin to decompose to create A- and B-rich phases having the compositions $c_e^*(T)$ and $c_{-e}^{**}(T) = (1-c_{-e}^*(T))$ given by equation II.6.

Continuum arguments [16] suggest that the mechanism of decomposition is sensitive to the location of the image point of the system relative to the spinodal curve. If the system is quenched to a point outside the spinodal on the A-rich side, the anticipated mode of decomposition is through the nucleation and growth of distinct particles of concentration $c_e^{**}(T)$ while, if the quench is to a point within the spinodal, the decomposition may happen through the continuous development of concentration waves. While the distinction between these two decomposition mechanisms is not as well defined in an atomistic model as in a continuum one[17], the computer experiments in the present research involved quenches to points outside the spinodal gap to preserve a clear nucleation-and- growth decomposition mechanism.

It should be noted that our simulation does not include the effect (or even the presence) of vacancies. The basic diffusion mechanism used is not the vacancy mechanism but

the exchange mechanism. This is only done for speeding up the simulation process, and the inclusion of vacancies is not beyond the limits of the model or code.

Also, the important effect of elasticity is completely ignored in this model. This is justifiable only at the very early stages when the surface energy is high. Unfortunately the effect of elasticity cannot be accounted for in an easy way due to its long range nature. Alternate methods are available, both for continuum and semi-continuum simulations, that include the elasticity effect.

SIMULATION TECHNIQUES AND CORRELATION WITH MODEL

We will first describe a simulation code following exactly the processes described in chapter 2, and then improvements over this code can be discussed.

First of all, the results (T_c, phase diagram) of the exact calculations of equilibrium properties are all for an infinite lattice. Since in the computer we can only use finite lattices, this will introduce boundary effects in these equilibrium properties.

In the simulation of an isolated system the whole system can be observed directly and there is no need to consider what happens outside. However for our case of an infinite system the computer observation of the kinetics of our finite lattice is just a simulated sampling of a finite group or sample of particles from the infinite system. The sample particles in the finite lattice interact with parti-

cles outside, and this interaction must somehow be incorporated into the simulation. The simplest means of allowing for the interaction is to consider the sample finite lattice to be replicated to fill space. The particles at or the near the boundary of the sample interact with the particles of the adjacent replicated samples. For the purposes of computing this interaction these outer particles may be taken as the equivalent inner particles of the actual sample. Since our model considers nearest neighbour interactions only, this representation of the infinite system should be adequate.

The imposition of this periodic structure on the infinite system has in fact replaced that part of the infinite system outside the sample by boundary conditions on the surface of the sample. This type of boundary conditions is generally referred to as Periodic Boundary conditions.

Having defined our basis as a finite lattice with periodic boundary conditions, we can now go on to describe

the simulation procedure.

Simple Monte Carlo Simulation:

The lattice is initially filled up randomly with the A and B atoms of a given composition. This is accomplished by initially setting all the sites to +1 and then setting a fraction c of the sites chosen randomly to -1. Here c is the fraction of B atoms, sites with +1 represent A atoms and sites with -1 represent B atoms. The initial random distribution represents equilibration at a very high temperature. [For statistical purposes, each time a different initial random distribution is chosen].

The Monte Carlo simulation then consists of the following steps[12]:

(1) choose and atom at random (from among all the atoms), say at location j.

(2) choose a neighbouring atom at random from among the nearest neighbours of j, say at location 1.

This establishes a randomly chosen atom pair j - 1 to be exchanged (or bond to be flipped).

(3) determine the exchange probability P_{j1}

$$P_{j1} = \frac{\exp(-\beta\Delta n_{j1})}{1 + \exp-\beta\Delta n_{j1})} \qquad \text{IV.1}$$

where

$\beta = 0.8814/T$

T = dimensionless reaction temperature

$= T_{real}/T_c$

$$\Delta n_{j1} = -\frac{1}{2}(\eta_1 - \eta_j)\left[\sum_i \eta_i - \sum_k \eta_k\right]$$

η_i = value of site i

where i = nearest neighbours of j

k = nearest neighbours of k

The temperature of the reaction is thus incorporated in out model through the probability P.

(4) Generate a random number R, $0 \leq R \leq 1$. Exchange j and 1 if $R \leq P$. In other words, exchange j and 1 with probability P.

(5) Repeat steps 1-4.

We see that in each trial one exchange is tried. As

exchanges proceed, the lattice structure changes dynamically towards the equilibrium structure. One trial per each lattice site measures one unit of time.* Thus by keeping track of the number of trials (time) the reaction can be followed in real time, and the kinetics can be studied.

This approach was used for studying ordering reactions as early as 1959[13], and has recently gained importance in the study of clustering reactions[14-19]. Whereas in the former case it was mainly used to study the equilibrium properties, in the latter case it is used to study the kinetics of clustering. Previous studies on this subject have been summarized in detail by Binder et al[7]. A recent study has employed this approach to study the kinetics of ordering reactions[20].

*Since the exchange probability of $\Delta n = 0$ exchanges is 0.5, the average time between such exchanges would be two time units. Considering the diffusion coefficient D (at the reaction temperature) in the limit of zero concentration of B atoms (where all the exchanges would be of $\Delta n = 0$) we see that for a square lattice, 1 time unit = $a^2 \times 8D$, where a is the lattice parameter.

Modified Monte Carlo Technique:

There are two basic drawbacks in the regular Monte Carlo method:

(1) It considers many unnecessary exchanges — those that lead to no change in the energy or microstructure.

(2) Since the exchange probabilities are all ≤ 1, a few trials are needed before an exchange occurs. Further as time increases, and as more and more atoms reach lower energy positions, the average jump probability goes down. From the programming point of view this means that more and more jumps have to be tried before one succeeds, and the simulation becomes very slow.

These drawbacks were overcome as follows : The first one was overcome by suitably modifying the program to avoid unnecessary exchanges by considering only those exchanges that lead to a change in microstructure — only AB bond interchanges need to be considered (with appropriate provi-

sion for a stochastic time variable).

The second drawback was overcome by observing that for each crystal structure there are only a few possible configurations of AB bonds, hence only a few possible values of Δn and hence only a few possible values of P. The possible jump configurations can thus be classified into types of identical exchange probability and selected for exchange directly, with probability weighted by the population of each type. That means, in each trial one exchange occurs. This method of simulation is much faster than the regular method.

In the square lattice there are seven different types of AB bond configurations and these are exemplified in Table I. The number of types of AB bond configurations possible in a few other crystal structures is shown in Table II.

In the following pages we give a brief description of the formulation of the model in a way amenable to fast com-

TABLE I. Bond Classification

Type of bond (i)	Example of configuration	Change in energy ΔE on exchanges/J	Probability of occurrence at $T = \infty$ and concentration C (N_i)	$N_i/\Sigma N_i$ for $C = 0.2$ ×
1	A B A-B-A-B A B	-12	$4C^4 (1-C)^4$	0.41
2	A B A-B-A-A A B	-8	$12[C^5(1-C)^3 + C^3(1-C)^5]$	5.2
3	A B B-B-A-A A B	-4	$12[C^6(1-C)^2 + C^2(1-C)^6] + 36C^4(1-C)^4$	23.4
4	B A A-B-A-A A B	0	$4[C^7(1-C) + C(1-C)^7] + 36[C^5(1-C^3 + C^3(1-C)^5]$	41.9
5	B A A-B-A-B B A	+4	$12[C^6(1-C)^2 + C^2(1-C)^6] + 36C^4(1-C)^4$	23.4
6	B A A-B-A-A B A	+8	$12[C^5(1-C)^3 + C^3(1-C)^5]$	5.2
7	B A B-B-A-A B A	+12	$4C^4(1-C)^4$	0.41

TABLE II.

Crystal Structure	Number of Types of AB Bonds
Square	7
Hexagonal	7
Simple cubic	11
Body centered cubic	15
Face centered cubic	11
Hexagonal close packed	11

puter simulation.

Exchange of a single atom pair:

Since exchanges of like atoms leave the microstucture unchanged, we need consider only exchanges involving pairs of unlike atoms. Let ΔE_α be the change in the total energy of the system if α^{th} unlike pair is interchanged; by equation II.3 $\Delta E_\alpha i$ is simply proportional to the net change in the number of AB bonds caused by the exchange. The probability that an exchange will be successfully accomplished in a single activation trial depends on the temperature and also on whether an activation berrier, ΔE^*, opposes the exchange. In the present work we treat a system for which $\Delta E^* = 0$.

An attempted atom exchange has two possible outcomes: a success, with relative Boltzmann probability

$$p_\alpha^s = \exp(-\Delta E_\alpha / T) \qquad \text{IV.2}$$

and a failure, with relative probability

$$p_{\alpha}^{f} = 1 \qquad \text{IV.3}$$

The normalized probability of exchange in a single trial is then

$$\begin{aligned} p_{\alpha} &= \exp(-\Delta E_{\alpha}/T)/[1+\exp(-\Delta E_{\alpha}/T)]^{-1} \\ &= [1+\exp(\Delta E_{\alpha}/T)]^{-1} \end{aligned} \qquad \text{IV.4}$$

For completeness we note that when the activation energy, ΔE^*, is non-zero and greater than ΔE_{α} a slightly different probability applies. Adopting the assumptions that $\Delta E^* >> \Delta E_{\alpha}$, and the E is a linear function of displacement along the configuration coordinate describing the exchange, and the ΔE^* has its maximum at the half-way point of the exchange, the relative probability for success becomes

$$p_{\alpha}^{s} = \exp-(1/T)[\Delta E^* + 1/2\Delta E_{\alpha}], \qquad \text{IV.5}$$

with which

$$p_{\alpha} = [1+\exp(1/T)(\Delta E^* + 1/2\Delta E_{\alpha})]^{-1} \qquad \text{IV.6}$$

Given the probability p_{α} that the α^{th} pair exchanges on a single attempt, the probability that no exchange has occured after j attempts is

$$p_{\alpha}(j) = (1-p_{\alpha})^{j} \qquad \text{IV.7}$$

Let the exchange trials occur randoomly in time with expected frequency per unity of time. Defining the dimensionless time

$$t^* = \nu t \qquad \text{IV.8}$$

the probability that there will be exactly j trials in time t^* is

$$p_j(t^*) = (j!)^{-1}(t^*)^j \exp(-t^*) \qquad \text{IV.9}$$

The probability that the α^{th} pair will not have exchanged after the time t^* is then

$$\begin{aligned} R_{\alpha}(t^*) &= \sum_{j=0}^{\infty} [(j!)^{-1}(t^*)^j \exp(-t^*)](1-p_{\alpha})^j \\ &= \exp(-p_{\alpha}t^*) \end{aligned} \qquad \text{IV.10}$$

provided that no other atom in the immediate vicinity of the α^{th} pair has changed in type, i.e., that ΔE_{α} remains constant over the interval t^*.

The lifetime of a configuration:

The exchange of an AB pair within the lattice will perturb the energies of atoms in its immediate coordianation

shell, and will hence change the exchange probabilities for AB pairs involving these atoms. The statistics of thermal activation are, therefore, simpler if the statistical element is taken to be the configuration of atoms over the lattice rather than the individual AB pair, where a configuration (q) is specified by giving the type of the atom, A or B, present at each lattice site. The successful exchange of any AB pair changes the configuration.

The lifetime of a particular configuration (q) may be easily computed. Let q contain N_{AB} binary pairs denoted $\alpha = 1 \ldots\ldots\ldots N_{AB}$. The probability that none of these pairs has exchanged in a time, t*, after the configuration is established, i.e., that the configuration survives for time greater than t*, is

$$R_q(t^*) = \prod_{1}^{N_{AB}} R_\alpha(t^*) = \exp(-\Lambda_q t^*) \qquad \text{IV.11}$$

where the activation parameter, Λ_q, is

$$\Lambda_q = \sum_{\alpha=1}^{N_{AB}} p_\alpha \qquad \text{IV.12}$$

The probability, $p_q(t^*)dt^*$, that the first exchange in the configuration q occurs during the time interval (t^*, t^*+dt^*) is governed by the function

$$\begin{aligned} p_q(t^*) &= \frac{\delta^*}{\delta t^*}[\Pi_q(t^*)] \\ &= \Lambda_q \exp(-\Lambda_q t^*) \end{aligned} \qquad \text{IV.13}$$

It follows that the expected lifetime of q is

$$\langle t^* \rangle_q = \Lambda_q^{-1} \qquad \text{IV.14}$$

with variance

$$\sigma_q^2 = \langle t^{*2} \rangle_q - \langle t^* \rangle_q^2 = \Lambda_q^{-2} \qquad \text{IV.15}$$

The transformation path and kinetics:

Equations IV.13 - IV.15 govern the lifetime of the configuration (q) without reference to the specific exchange which occurs. The probability that a particular pair, α, is that which exchanges first may be easily computed (or inferred) and is

$$\eta_\alpha(q) = p_\alpha/\Lambda_q \qquad \text{IV.16}$$

The occurance of the exchange creates a new configuration, q+1, and resets the statistical clock. The lifetime of con-

figuration q+1 is then determined by using the appropriate value of the activation parameter, Λ_{q+1}, in equations IV.13 - IV.15.

Let the solution evolve through a sequence of r pair exchnages. Each exchange establishes a new rest configuration of the solution. The sequence, q=1.....r, defines the "transformation path". The statistical process through which the transformation path is chosen may easily be shown to be Markovian[22] from which it follows that the expected time to pass through the configuration q=1.....r is

$$\langle t^* \rangle = \sum_{q=1}^{r} \langle t^* \rangle_q \qquad \text{IV.17}$$

with standard deviation

$$\sigma^2 = \sum_{q=1}^{r} \sigma_q^2 \qquad \text{IV.18}$$

If r is large the times are normally distributed according to the relation

$$p(t^*) = (2P_i\sigma_q^2)^{-1/2} \exp-[(t^*-\langle t^* \rangle)^2\sigma_q^2] \qquad \text{IV.19}$$

where p(t*) is the distribution function for the time to

reach the r^{th} configuration.

It follows from equations IV.17 - IV.19 that the kinetics of evolution of the model binary solution are determined once the sequence of confugurations through which the solution passes is known. Each of these differs from its predecessor through a single binary exchange which is determined statistically by equation IV.16. Hence a computer simulation of the evolutionary process need only determine the probabilities, p_α, and their sum, Λ_q, for each configuration along the evolutionary path. Given a particular configuration, a random number may then be chosen and used in conjunction with equation IV.16 to select a specific AB pair for exchange.

Specification to the Binary Ising Lattice:

The computation of the exchange probabilities, p_α, and their sum, Λ_q, is particularly simple when the model system is a binary Ising lattice, since the energy of an atom in a

binary Ising lattice is determined by the identity of its nearest neighbors. The exchnage energy, ΔE_α, for a pair in an Ising lattice may have one of only a few discrete values, which correspond to the energetically distinguishable ways of choosing the nearest neighbours of the A and B atoms in the pair. In a two dimensional square lattice, for example, there are only seven possible values of ΔE_α. These are presented in Table I, together with their occurance possibilities in a random configuration of mean concentration, c. It may be shown in general that the number of distinct types of A-B pairs is odd since, if a particular exchange causes the energy change ΔE_α, its reverse will change the energy by $-\Delta E_\alpha$ and since there is always a possible configuration of the pair for which $\Delta E_\alpha = 0$.

Let there be m energetically distinguishable types of AB pairs in an Ising lattice. Let ϵ_i be the exchange energy for the i^{th} type; ϵ_i is an integer if measured in units of the interaction parameter, J. The exchange probability for

the i^{th} pair type is then

$$P_i = [1+\exp(\epsilon_i/T)]^{-1} \qquad \text{IV.20}$$

when T is also given in units of J/k. The probabilities P_i are functions of temperature only.

The number of pairs of type i in the q^{th} configurations, $N_i(q)$, may be expressed in terms of the energy, $\epsilon(q)$, of the configuration II.3:

$$N_i(q) = N\epsilon(q)F_i(q) \qquad \text{IV.21}$$

where $F_i(q)$ is the fraction of the AB pairs which is of type (i). The activation parameter, Λ_q, may then be written

$$\begin{aligned} \Lambda_q &= \sum_{i=1}^{m} P_i N_i(q) \\ &= N\epsilon(q) \sum_{i=1}^{m} P_i F_i(q) \end{aligned} \qquad \text{IV.22}$$

Since $\langle t^* \rangle_q = \Lambda_q^{-1}$, it follows that the mean residence time in the configuration q varies inversely with the size of the system, N, and with its energy, $\epsilon(q)$.

As the solution approaches asymptotically to its (dynamic) equilibrium state, the energy will approach its

equilibrium value, $\epsilon_0(T)$, and the pair fractions will approach asymptotic values, $F_i^o(T)$, which are functions of temperature only. In this case Λ_q takes only values near to the equilibrium value

$$\Lambda_0(T) = NG_0(T)\Sigma P_i F_i^0(T) \qquad \text{IV.23}$$

If, as we shall see is often the case, the pair fractions approach their asymptotic values before the energy is equilibrated, then the activation parameter subsequently obeys the simple relation

$$\Lambda_q = (\epsilon_q/\epsilon_0)\Lambda_0) \qquad \text{IV.24}$$

and the activation time becomes simply proportional to the inverse of the energy.

The probability that the first pair to exchange in the q^{th} configuration is of type (i) is given by

$$\begin{aligned} \eta_i(q) &= N_i(q)P_i/\Lambda_q \\ &= P_i F_i(q)/\Sigma P_i F_i(q) \end{aligned} \qquad \text{IV.25}$$

which becomes configuration-independent when the pair fractions have relaxed into their asymptotic values. Each particular pair of type (i) is equally likely to be the pair

exchanged.

Topological Representation of Lattices:

The basic computer software has only the capabilities of representing one dimensional, two dimentional square or three dimensional simple cubic lattices directly. Alternate methods need to be found for the representation of other lattices.

As an example consider the representation of the (100) plane of an FCC system in the computer. The easiest way is to have a two dimensional array, with alternate words filled with 1's and 0's, as shown pictorially in Figure 2. The grid of 1's now represents the (100) plane of FCC, and the grid of 0's is neglected. This way of representation is one possible way but certainly not the most efficient. For example a lot of computer memory, 50% of the lattice in this case, is wasted. Further, recognition of a row or column without referring to it as "odd" or "even" becomes diffi-

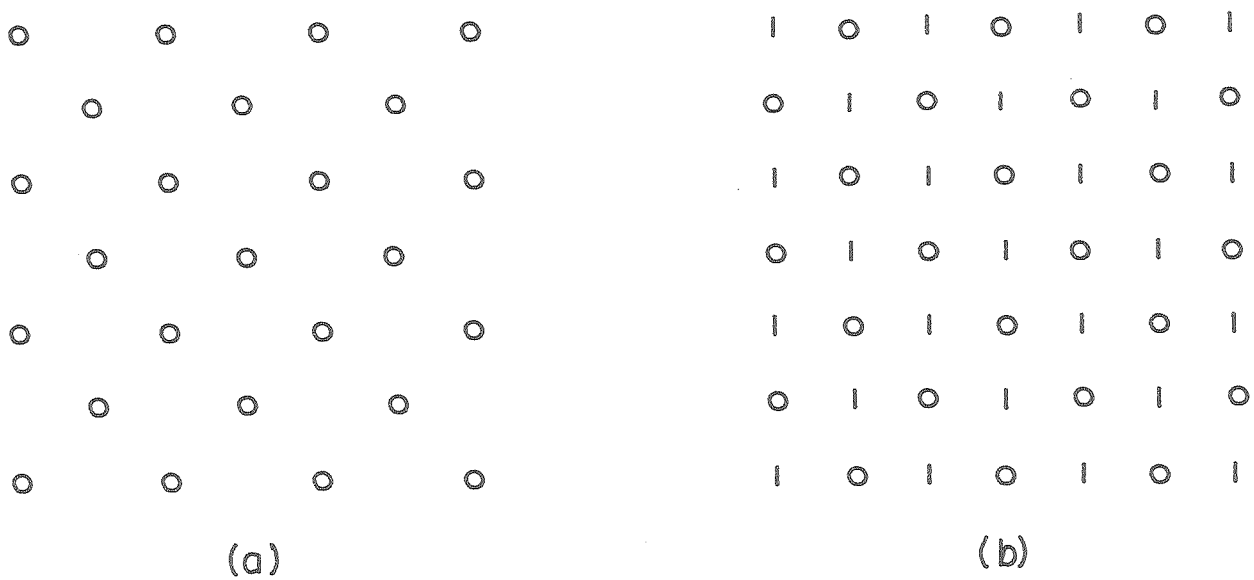

Fig.2. A possible representation in the computer (b) of the (100) plane of an FCC system.

cult. Also there are other problems associated with having meaningful boundary conditions.

These problems can be overcome by means of certain topological transformations which transform more complex lattices into equivalent basic one dimensional, two dimensional square or three dimensional simple cubic lattices.

The topological transformation of the two dimensional hexagonal lattice into the equivalent square lattice is shown in Figure 3. When the simulation has proceeded, and a microstructure of the lattice is needed, an inverse topological transformation on the equivalent square lattice yields the corresponding triangular lattice.

From the simulation point of view it takes much less computer time to reference a one dimensional array than a two or three dimensional arrays. This makes it worthwhile to transform the two or three dimensional arrays into one dimensional lattice representations. The transformation of

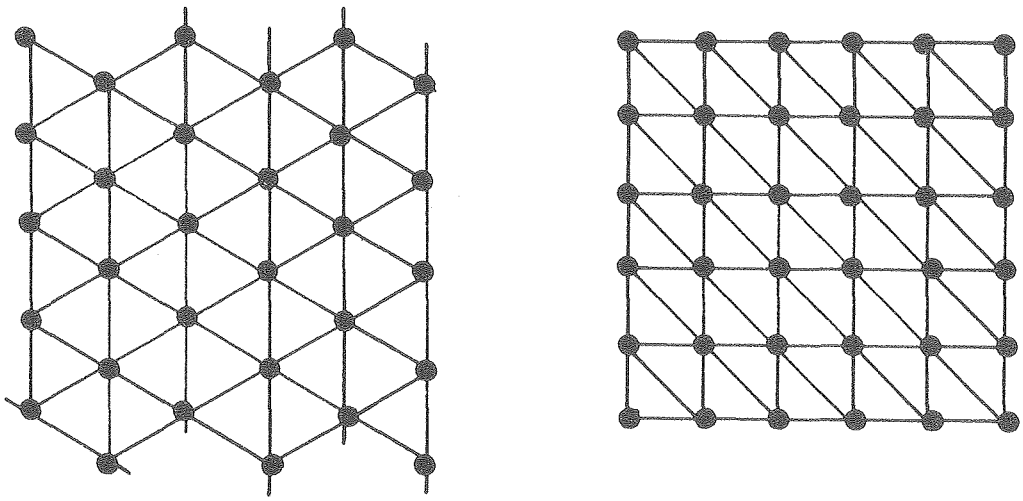

Fig.3. Topological transformation of the two dimensional hexagonal lattice into an equivalent square lattice.

a square lattice to one dimensions is very straightforward, as shown pictorially in Figure 4. This seemingly simple transformation made the code as much as 50% faster in execution, including the extra time taken for the transformation.

The transformation of the hexagonal lattice is accomplished in two steps. First it is transformed into an equivalent square lattice and then into an equivalent one dimensional lattice.

An example of topologically transforming an FCC lattice into an equivalent simple cubic lattice is shown in Figure 5. The simple cubic lattice is then transformed into the corresponding equivalent square lattice and then transformed again into the topologically equivalent one dimensional lattice.

This way of transforming all lattices into their equivalent one dimensional lattice representation has an important use. This has made it possible for writing an

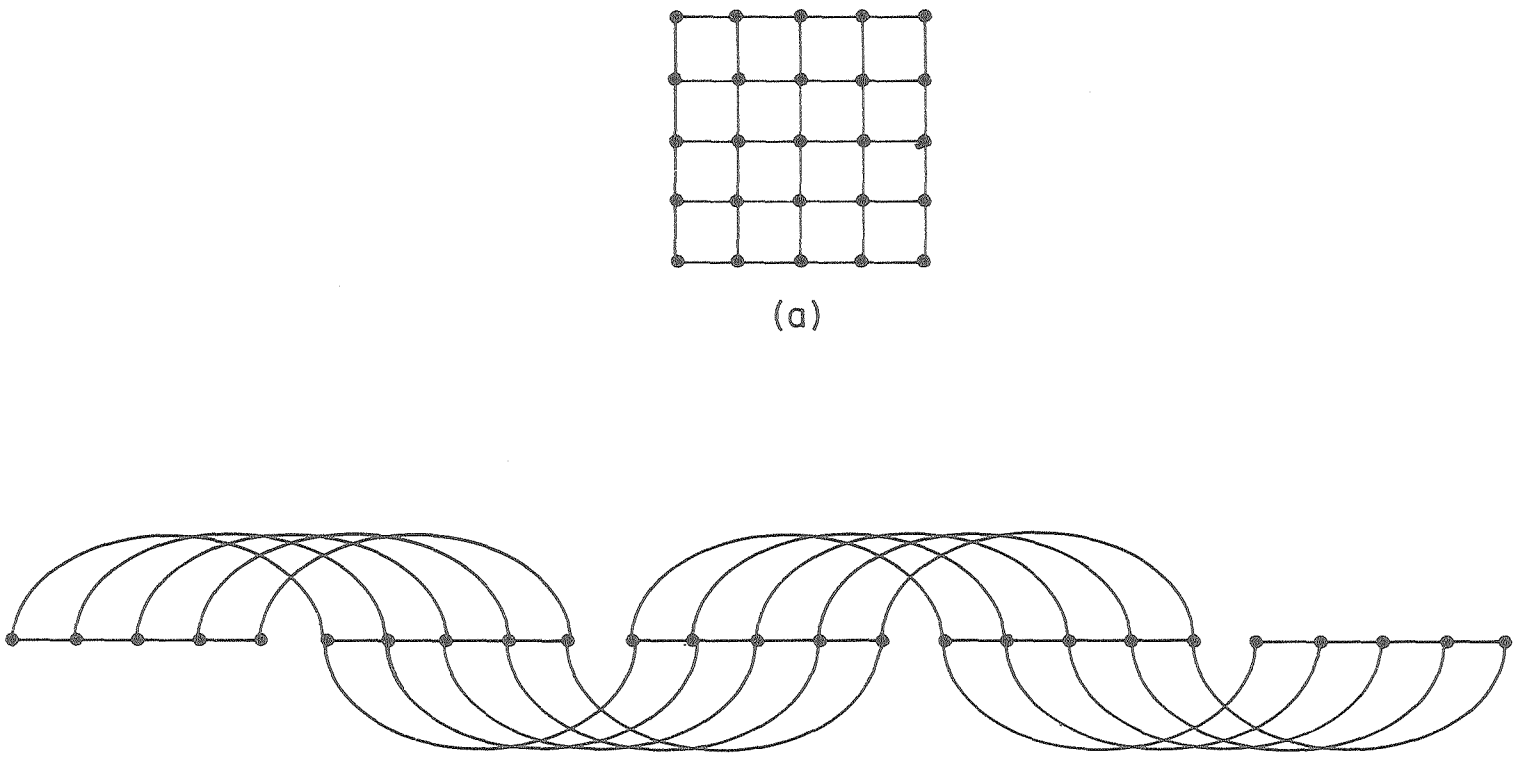

XBL 794-6145

Fig. 4. Transformation of a square lattice into a topologically equivalent one dimensional lattice.

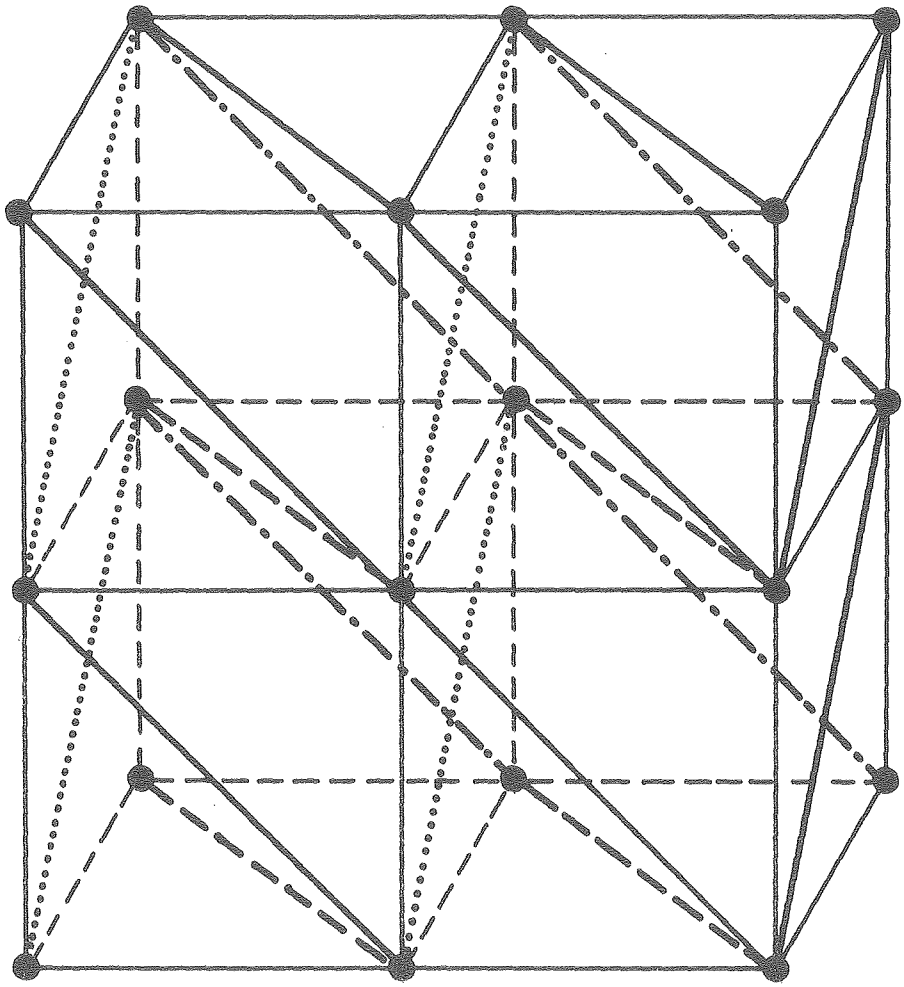

XBL 794-6143

Fig.5. Transformation of an FCC lattice into a topologically equivalent simple cubic lattice.

universal code which can perform simulation experiments on many different crystal lattice structures.

The Flow Chart of the code is shown in Figure 6.

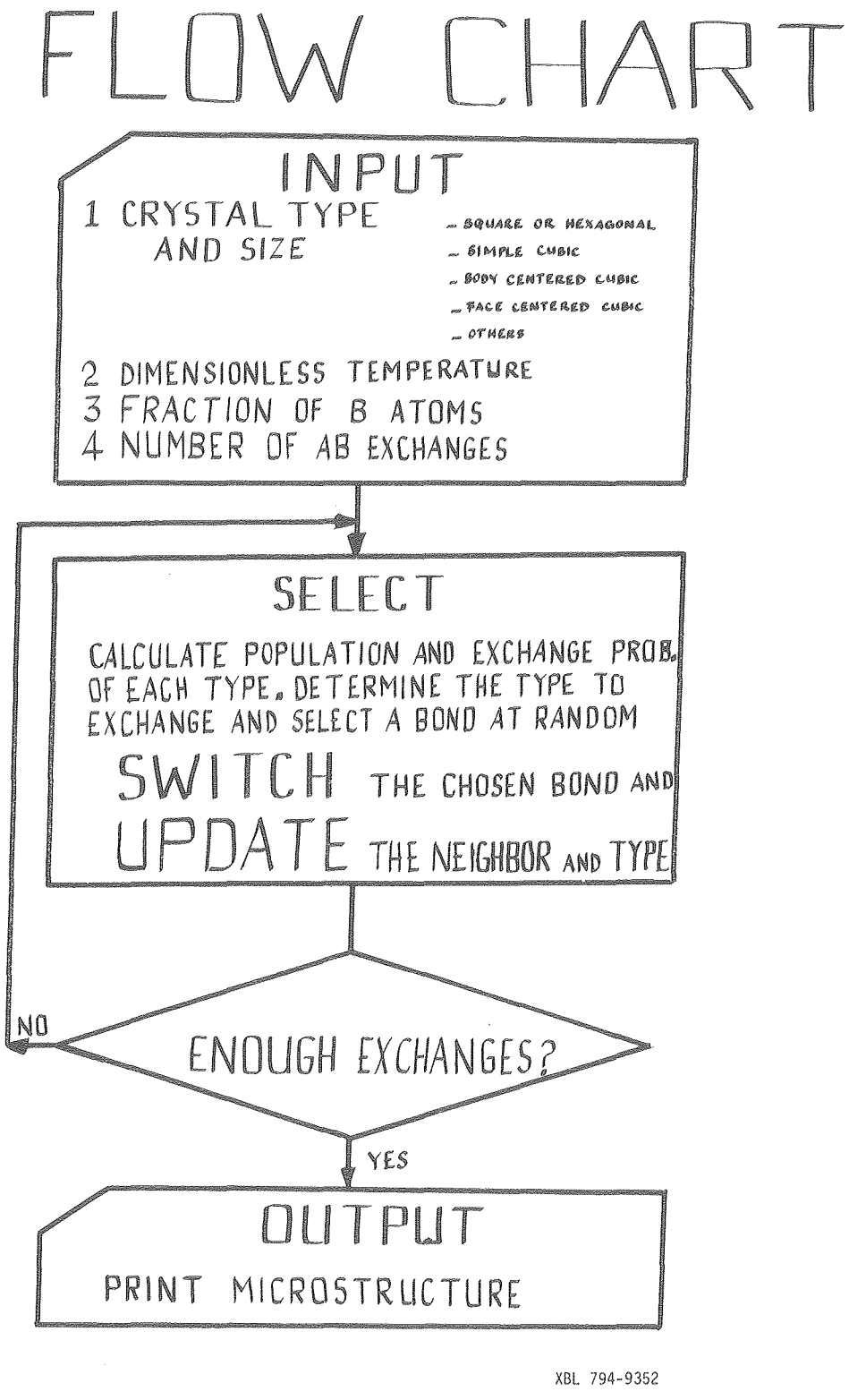

Fig. 6. Flow chart of the computer code.

RESULTS AND DISCUSSIONS

Figure 1 shows the phase diagram of a binary Ising lattice indicating the points of simulation reported here. Most of the simulations for square lattice were conducted on a 80 x 80 or 120 x 120 atom lattices, and for hexagonal lattice on 80 x 80 atom lattices. The data taken during the simulation included plots of the microstructure, and of the energy, the mean cluster size, and the pair type fractions as functions of time.

Equilibrium

The equilibrium, or asymptotic state of the binary Ising lattice was studied as a function of temperature by aggregating the B atoms into a square in the center of the array and letting the aggregate relax through atom exchanges at the temperature of interest until the energy and the pair type fracctions became sensibly independent of time. Examples of the equilibrium configurations obtained in this way

are shown in Figure 7. The values of the energy, activation parameter, and the pair type fractions obtained are presented for the several temperatures tested in Table III.

It will be noted from Figure 7 that the initial square is essentially preserved at low temperatures, through there is some roughening of the periphery of the square which, as expected, is most pronounced at the corners. At very low temperatures the equilibrium defect density is too small to be represented in an array of the size used here and no true equilibrium is obtained. At higher temperatures ($T>0.5T_c$) the surface becomes progressively rougher and solute atoms are seen in significant population both in the B-rich square and within the A-rich matrix.

It is also clear from the micrographs shown in Figure 7 that, at least for $T\leq 0.9T_c$, the vast majority of the AB bonds present in the system are located in the interface of the B-rich square; relatively few are associated with solute atoms in the two bulk phases. The equilibrium values of the

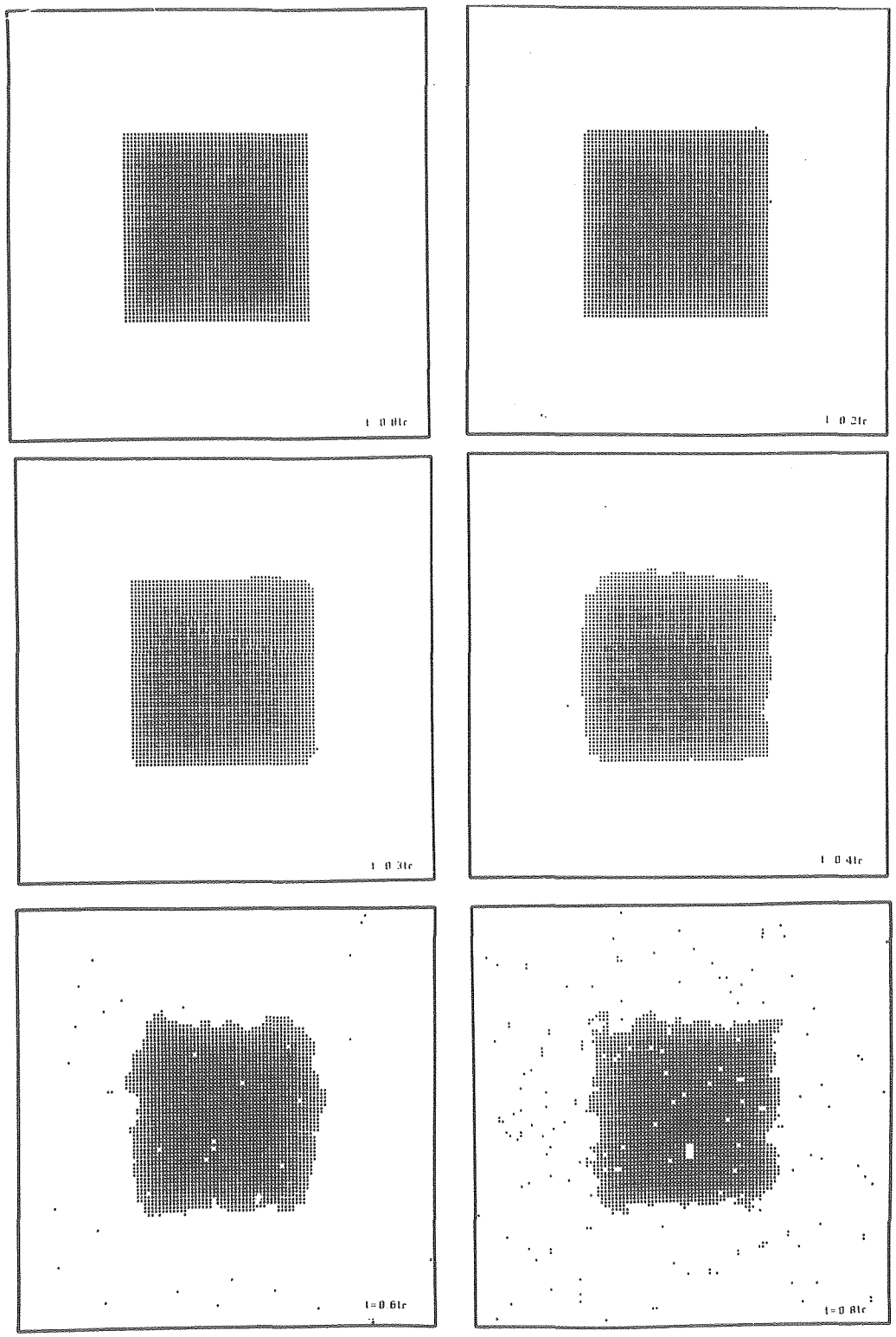

XBB 796 07951

Fig.7. Equilibrium structure of a 114*114, 20% square lattice at different temperatures.

pair type fractions presented in Table III are hence associated with, and determined by, the equilibrium of the interfacial region.

The Kinetics of Precipitation and Coarsening:

The kinetics of evolution of a square 120x120 Ising lattice which initially contains a random distribution of B atoms, C_B = 0.2, are given in Figures 8 and 9, and in Tables IV and V. Figure 8 contains plots of the average cluster size <n> as a function of time and temperature. For the purposes of this plot, a cluster is defined to be a semi-compact group of five or more atoms. Figure 9 shows similar plots of the change in excess energy $\langle \epsilon - \epsilon_\infty \rangle$, with time and temperature, where the reference values $\epsilon_0(T)$ are taken from Table III. Most of the curves in both figures contain two segments having nearly constant slope. The slopes of these segments are presented in Tables IV and V. The slopes of the short-time segments are compared to the prediction by Binder[6] for coarsening through the direct coagulation of

TABLE III.

PROPERTIES AT EQUILIBRIUM

T/T_c	$E\alpha$	$\log (1/F_i)$							$\sum_{i=1}^{7} F_i P_i$
		i=1	i=2	i=3	i=4	i=5	i=6	i=7	
0.2	0.016	11.5	8.9	5.4	1.72	1.54	1.25	0.05	0.0095
0.3	0.0163	7.7	6.1	3.8	1.63	1.27	0.95	0.09	0.012
0.4	0.018	6.0	4.4	2.8	1.34	0.87	0.57	0.26	0.027
0.6	0.035	4.6	3.1	1.9	0.47	0.63	0.59	0.80	0.193
0.8	0.072	4.0	2.7	1.6	0.31	0.60	0.80	1.20	0.30

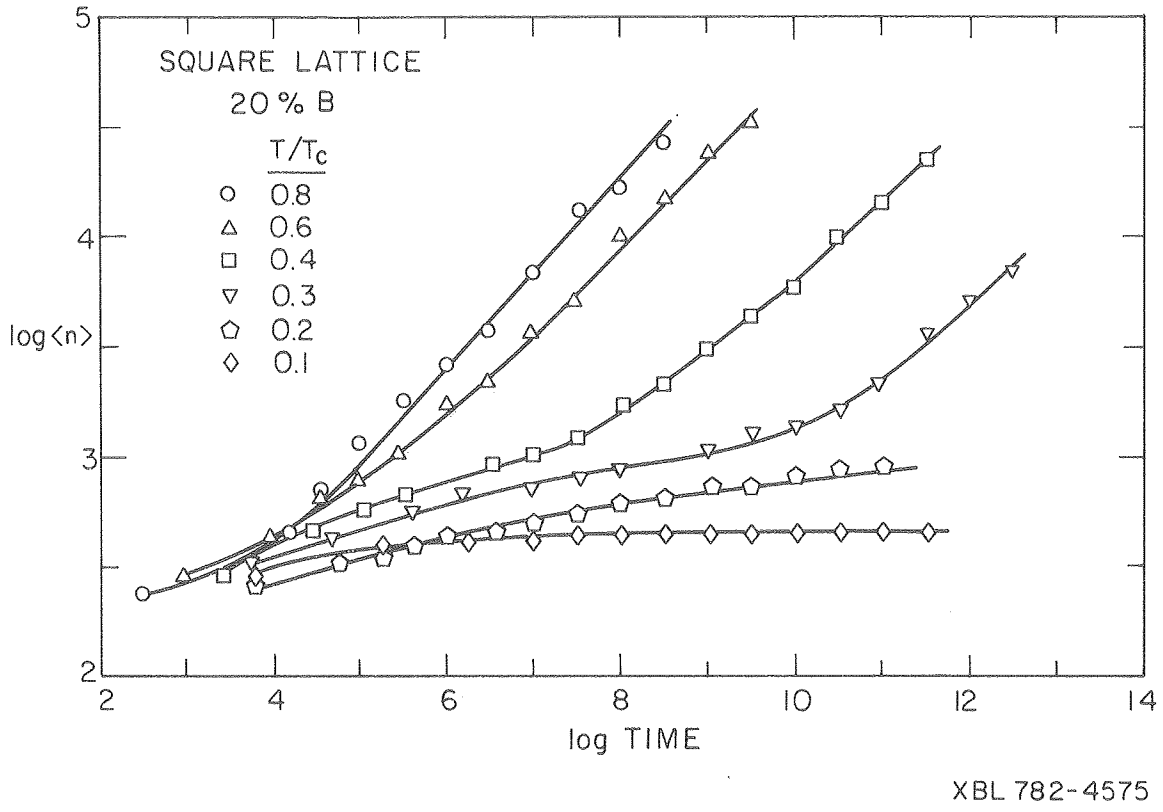

Fig. 8. Plots of average cluster size <n> vs. time for a 20% B alloy at various temperatures. Note that the same dimensionless diffusivity is used for all the temperatures.

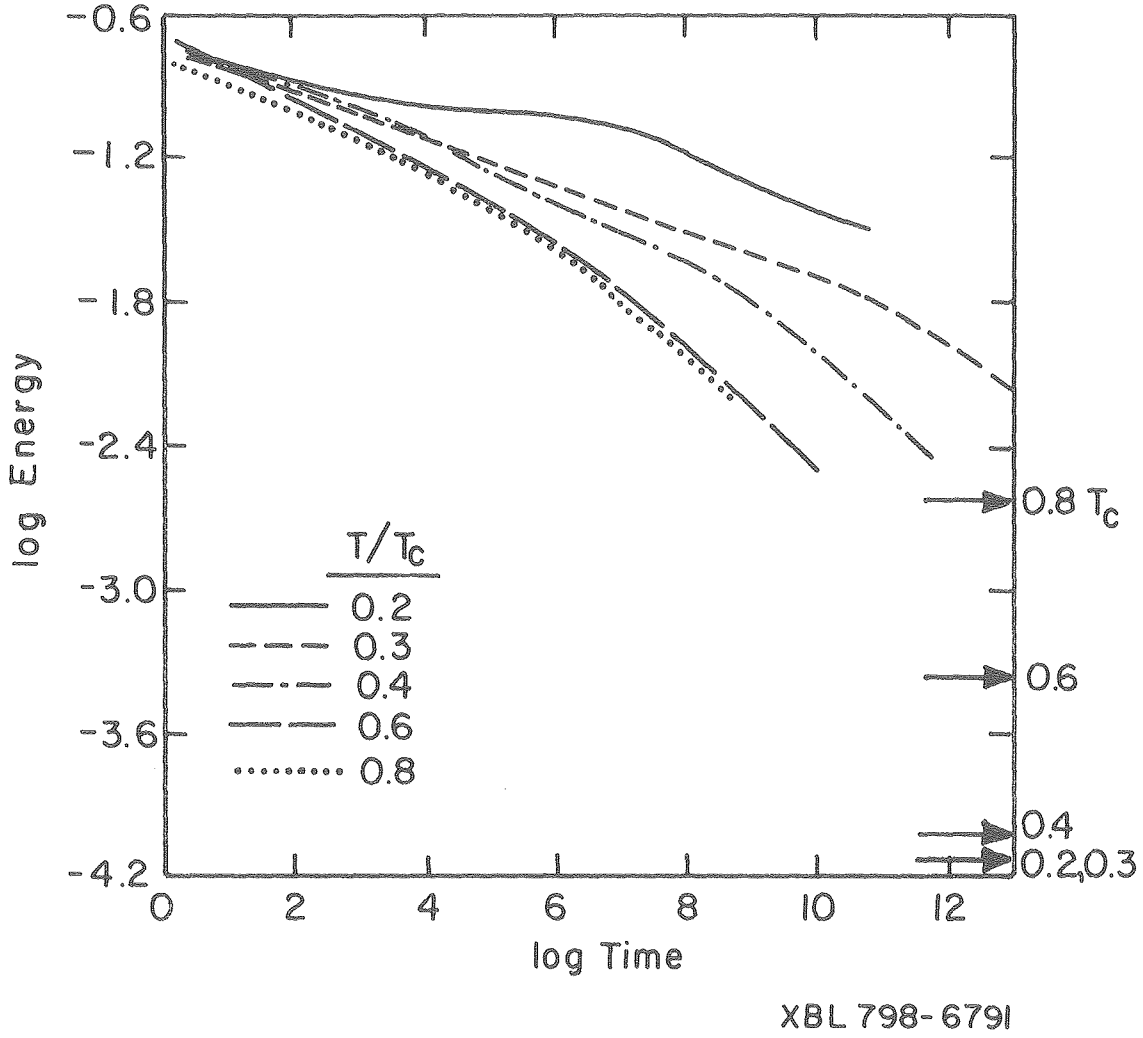

Fig.9. Plots of excess energy $\langle \epsilon - \epsilon_\infty \rangle$ vs. time for a 20% B alloy at various temperatures.

TABLE IV. Exponent a of $\langle \eta \rangle = t^a$

	$0.3T_c$	$0.4T_c$	$0.6T_c$	$0.8T_c$
20%B (square lattice)				
LS	0.38	0.40	0.48	0.53
Intermediate	0.10	0.13	--	--
Binder	0.24	0.27	0.27	0.30
10%B (square lattice)				
LS	0.40	0.46	0.48	0.67
Intermediate	0.20	0.20	--	--
Binder	0.25	0.26	0.29	0.37
20%B (hexagonal lattice)				
LS	--	0.53	0.35	0.39
Intermediate	--	0.18	--	--
Binder	--	0.28	0.31	0.31

TABLE V. Exponent b of $\langle \varepsilon - \varepsilon_\infty \rangle = {}^{-b}$

	$0.4T_c$	$0.6T_c$	$0.8T_c$
20% (square lattice)			
LS	0.26	0.26	0.27
Intermediate	0.12	--	--
Binder	0.16	0.15	0.16
10%B (square lattice)			
LS	0.32	0.30	0.31
Intermediate	0.12	--	--
Binder	0.18	0.17	0.16

clusters. The slopes of the long-time segments are compared to the prediction by Lifshitz and Slozov[3] for coarsening through single-atom diffusion. The agreement appears reasonable, but is inexact.

The results of two other series of simulations are also shown. Experiments on square arrays having C_B - 0.1 yielded reaction curves similar to those shown in Figures 8 and 9. The slopes of the straight line segments of these curves are included in Tables IV and V. The precipitation and coarsening reaction in an 80*80 lattice of hexagonal symmetry with C_B -0.2 was also simulated to indicate the influence of lattice geometry. A plot of the mean cluster size as a function of time and temperature for this case is included as Figure 10.

Mechanistic Interpretation:

1. Basic Coarsening Reaction

Our results indicate that in the most general case the

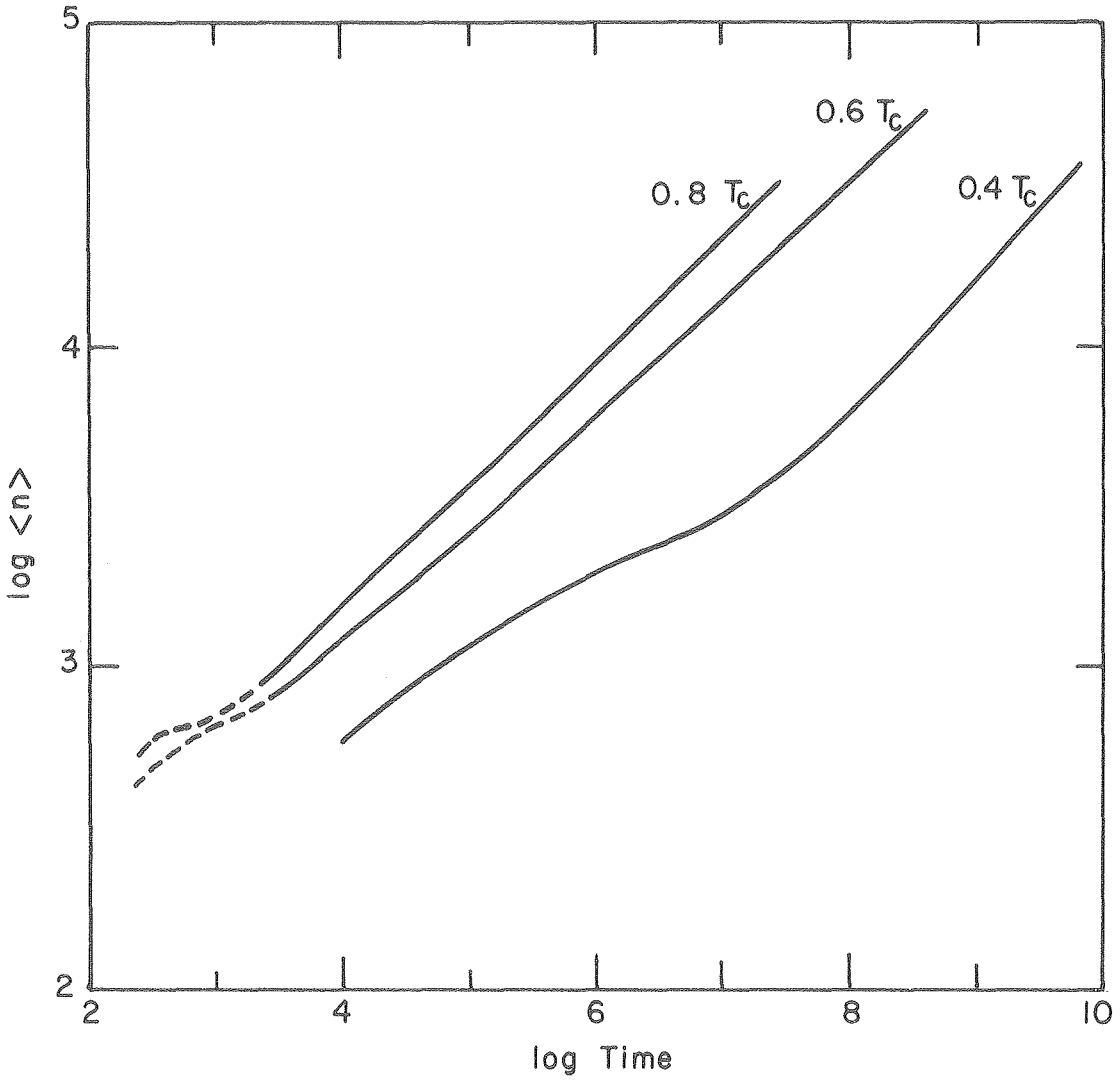

Fig.10. Plots of average cluster size <n> vs. time for a 80*80 hexagonal lattice of 20% B concentration.

precipitation and coarsening reaction follows four stages.

(a) Initial Relaxation: Soon after the quench from the infinite temperature, the system tends to relax to a lower energy state. The solution is decomposed into A-rich and B-rich phases and precipitation occurs. An example of this stage of the reaction is shown in Figure 11. Figure 11a shows the initial random configuration of a 20% B atom lattice, and Figure 11b shows the configuration after relaxation for 89 time units at $0.8T_c$. [The location of A atoms are left vacant and the locations of B atoms are represented by dots]. Defining the precipitate to be a cluster of B atoms connected by nearest neighbor bonds, we see that in Figure 11b most of the B atoms have joined one or the other of the precipitates. Monomers and transient clusters such as dimers and trimers can be interpreted as dissolved in the matrix and show nearly equilibrium concentrations even at this early time. In fact it can be said that the phase separation reaction, as dictated by the phase diagram is

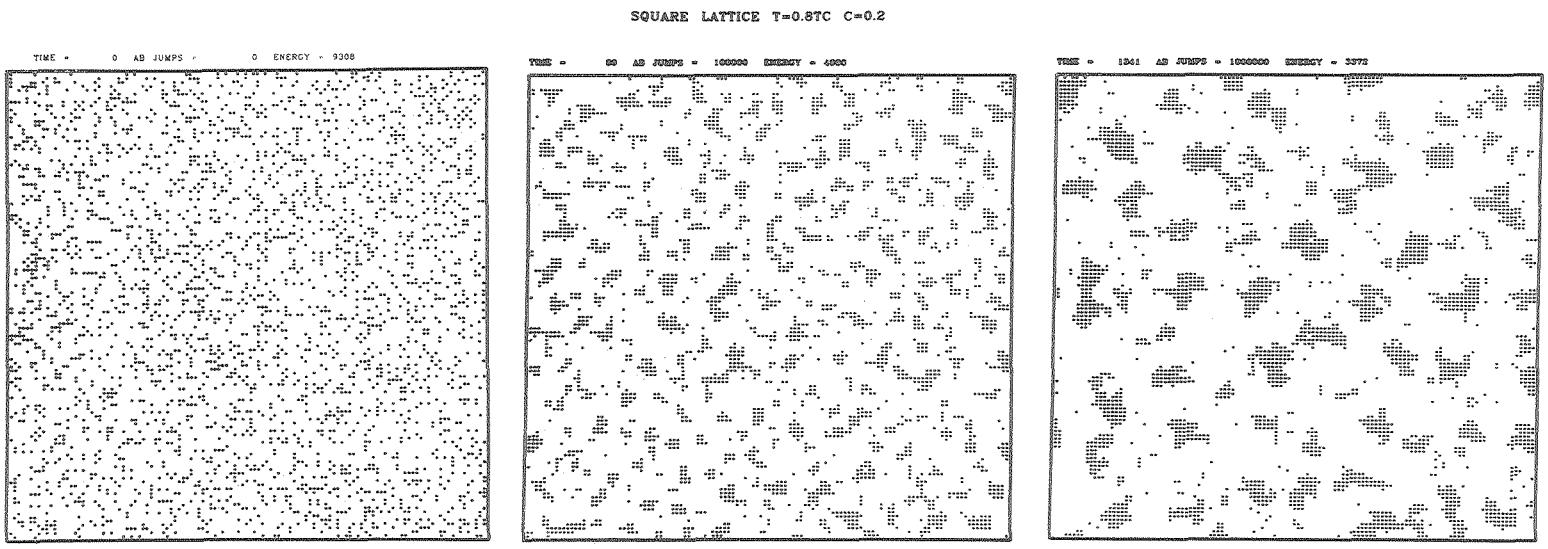

Fig.11. Time evolution of a 120*120 square lattice of 20% B concentration at $0.8T_c$. (a) Initial random configuration; (b) configuration after 89 time units and (c) configuration after 1341 time units.

XBL 7810-12103

essentially complete at this stage. This is seen in Table VI. For comparison see Figure 11c which is a late time picture.

Once the phase separation reaction is essentially complete the dominant reaction becomes particle coarsening, a process which is initially dominated by the diffusion and direct coagualation of the clusters as suggested by Binder[6]. Examples of cluster coagulation during the early stages of coarsening are shown in Figure 12, which contains four "snap-shots" of the configuration of the square lattice of C = 0.1B during reaction at $0.3T_c$.

Cluster coagulation has its source in the mobility of distinct clusters. A motion of the center of mass of the cluster may be caused either by the movement of atoms over its surface, which is expected to be the primary mechanism at low temperature or by the dissolution and re-depositions of atoms which should be dominant at higher temperature. The mobility of a cluster decreases with its size with the

TABLE VI.

Concentration	T/T_c	Equilibrium Fraction of B atoms in the matrix (from phase diagram)	Concentration in matrix after 10,000 jumps
0.1	0.8	0.2129	0.2
0.1	0.6	0.056	0.06
0.1	0.4	0.0028	0.003
0.1	0.3	0.00179	0.002
0.2	0.8	0.12876	0.14
0.2	0.6	0.025	0.025
0.2	0.4	0.001276	0.0013

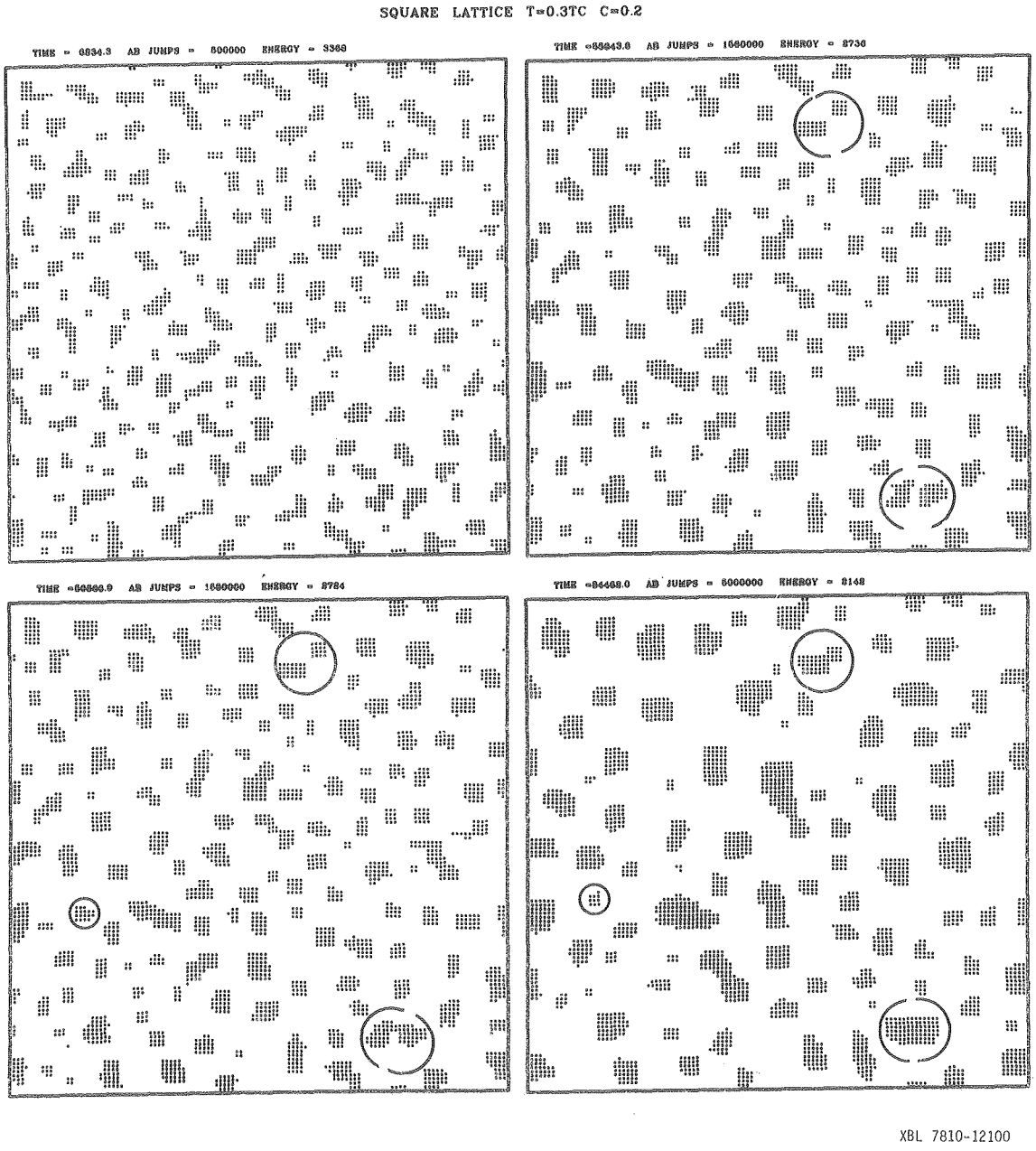

Fig.12. Snapshots during the time evoultion of a 120*120 square lattice of 20% B concentration at 0.3 T_c showing cluster diffusion and coagulation mechanism for example in regions marked with big circles. Notice also the atom by atom transfer mechanism, such as in the area marked with the small circles.

result that the contribution to the overall coarsening rate due to cluster coagulation decreases in importance relative to that from normal Ostwald ripening, which eventually becomes the dominant mechanism.

Binder's[6] analysis of coarsening through the cluster coagulation mechanism suggests that the rate of coarsening will be logarithmic (equation I.3) with a time exponent whose value depends on the dominant mechanism of cluster mobility: 0.4 for surface diffusion and 0.5 for volume diffusion control. The simulation results show nearly logarithmic behavior during the cluster coagulation phase, and indicate a somewhat higher slope at higher temperature, which closer analysis suggests may be associated with an increasing contribution of volume diffusion to cluster mobility. The slopes are, however, somewhat smaller than what Binder predicts. The source of the discrepancy may lie in the discrete lattice. Particularly in the case of a square lattice, in which the nearest neighbors of a lattice

site are not nearest neighbours of one another, the lattice imposes constraints on atom mobility over the surface of small clusters which causes surface diffusion to be more difficult than continuum analysis would suggest. The discrete lattice constraint is less important when the lattice is hexagonal, and our simulation data (Figure 10) does show a more pronounced coarsening due to cluster coagulation, at a higher time exponent, in this case.

(c) Transition stage: This stage is characterized by a very small coarsening rate, especially significant at low temperatures. The reaction rate is basically controlled by the dissolution of atoms at precipitate surfaces. The seven different types of bonds (see Table I) reach constant relative populations $N_i/\Sigma N_i$ at the end of the transition stage. As an example, the variation of $N_4/\Sigma N_i$ with time is plotted on Figure 13, superimposed on the <n> vs time plot. These constant relative populations depend on the temperature, and at infinite temperature they depend only on concentration,

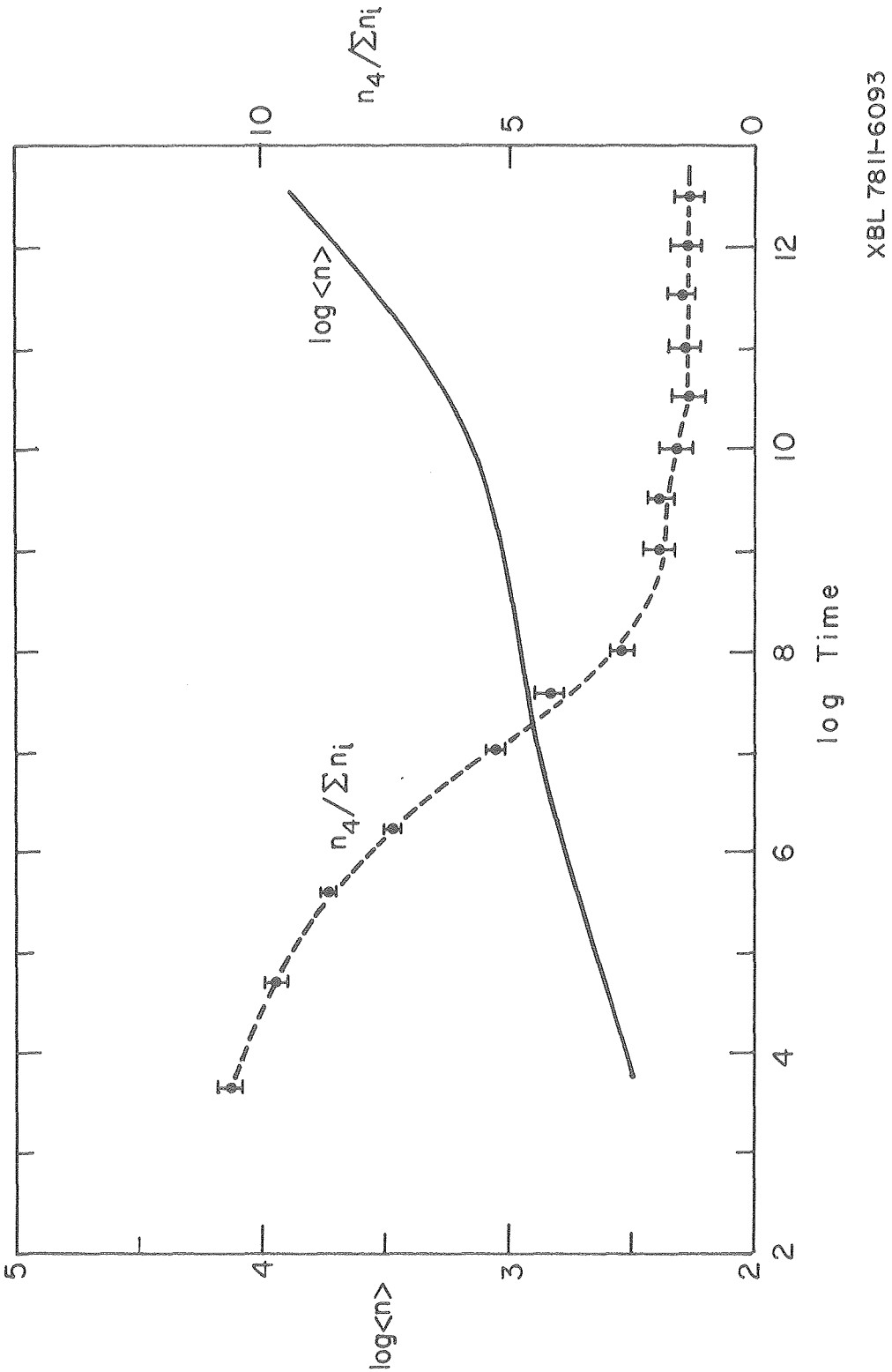

Fig.13. Plot of average cluster size <n> vs. time for a 120*120 square lattice of 20% B concentration at a reduced temperature of $0.4T_c$. Also shown is the corresponding values of relative bond population of bonds of type 4 (see Table I).

as listed in Table I. Figure 14 shows the relative populations of all the seven types of bonds for a temperature of $0.4T_c$ and it is seen that they all tend to reach asymptotic levels as the transition stage starts to end. From this figure we can also conclude that the Binder reaction is basically occuring at a time when the bonds have not reached their asymptotic relative populations, and these relative populations are dynamically changing.

(d) Lifshitz and Slozov coarsening: This is the usual Ostwald ripening occuring through atom by atom transfers from clusters to clusters, with diffusion through the matrix controlling the rate. This mechanism becomes predominant in the very late stages of the coarseing reaction and occurs at a rate faster than either (b) or (c).

A clearcut distinction into these four stages is not possible and there is always an overlap. The extent of overlap is temperature dependant and will be treated in a later section. The precipitates in the early stages are

clearly non-spherical, and there exists a tendency towards spherodization as the reaction proceeds. Long thin clusters sometimes split into two or more in their efforts to spherodize. Sometimes a group of B atoms separate from a big cluster. These can then either redissolve in the matrix and redeposit on the surrounding clusters (LS mechanism) or can diffuse as a unit to join another cluster (Binder mechanism). This type of overlap of mechanisms occurs almost at all times. Although the predominant mechanism is determined by the average cluster size, the path chosen by a particular cluster depends on its own size and its local environment.

2. Effect of Temperature

(a) Effect on overall kinetics: In this section we discuss the modifications in the general four stage coarsening scheme effected by temperature. Figure 8 shows the plots of average cluster size <n> vs time at various temperatures for a 20% B atom alloy of 14400 atoms. Table IV and V gives the exponents a and b (equation I.1) at early,

intermediate and late times. Whereas at medium temperatures all the four stages are present, at high temperatures stage 3 is absent, and at very low temperatures stage 4 is absent. At higher temperatures the change from Binder's to LS mechanism is rather gradual, both mechanisms overlapping over a wide range of times. At lower temperatures the two mechanisms are completely separated by a region of stage 3 with a slope lower than for either of the mechanisms; at short times 80% of the reaction is cluster diffusion and coagulation, and at long times 80% of the reaction is LS type. Further, the dimensionless time taken to reach steady-state or LS coarsening increases as we go down in temperature, with stage 3 extending further and further.

All these changes in kinetics with temperature stem from changes in (i) cluster geometry, (ii) relative jump probability, and (iii) matrix concentration of solute.

(i) Cluster geometry:

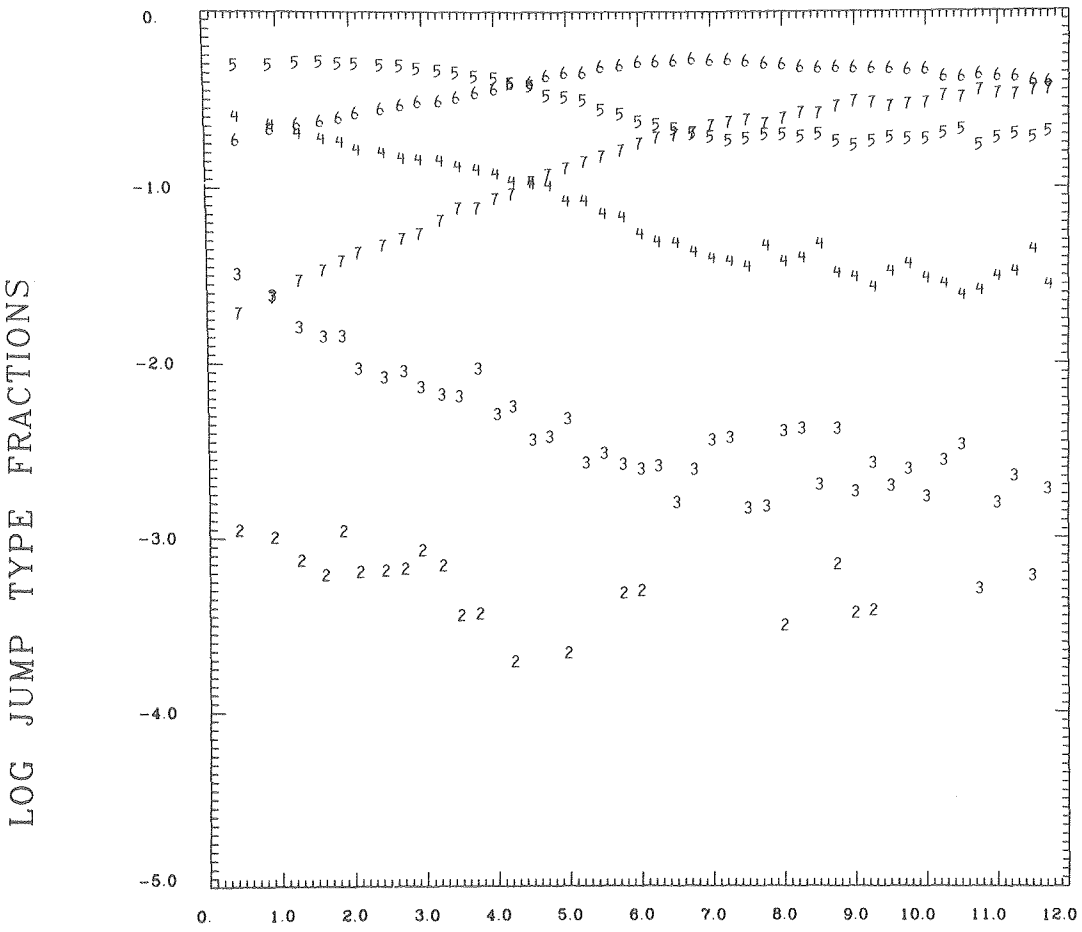

Fig. 14. Plot of bond-type fraction vs. time for a 20% B alloy of 0.4 T_c.

At high temperatures the clusters are rather diffuse, and seldom possess well defined boundaries until they reach larger sizes. The clusters at low temperatures are on the other hand much more compact. Figures 15 a and 15b show the microstructures of a 20% B atom alloy in a square lattice at low ($0.4T_c$) and high ($0.8T_c$) temperatures. At roughly the same time after quench (since we use dimensionless diffusivities, the actual times at the low temperature would be much longer), the critical cluster size (which keeps on changing with time) is much smaller at the low temperature, and this leads to a high population of small sized clusters at $T=0.4T_c$ (Figure 15a). Further for $0.4T_c$ the equilibrium concentration in the matrix is much lower, as should be evident from the phase diagram.

More localized effects are observed at the lower temperatures. Each cluster tries to expose the face of lowest energy and this results in most of the clusters having (100) faces (which have only one exposed bond per surface atom).

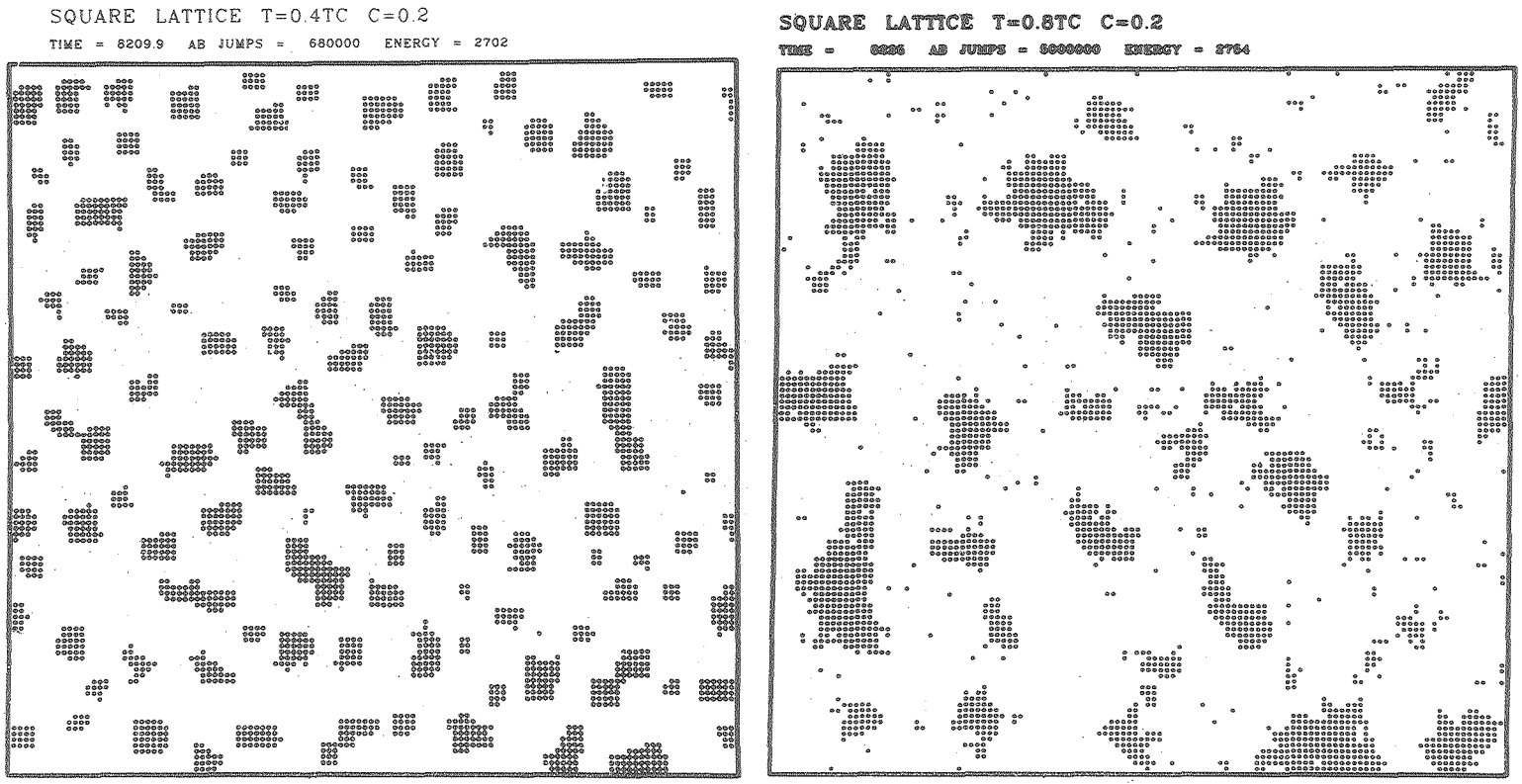

XBL 7810-12102

Fig.15. Microstructure of a 20% B alloy at roughly the same time after quench to (a) $0.4T_c$ and (b) $0.8T_c$.

The average number of surface bonds per surface atom for an average cluster size of 60 atoms is about 1.6 for $0.8T_c$ and only 1.35 for $0.4T_c$. These numbers are for surfaces met with in our simulations. More precise numbers at any temperature can be obtained by studying the equilibrium profile of an initially straight infinite edge, in equilibrium with the equilibrium solute concentration at that temperature (obtained from the phase diagram).

The geometry of clusters at low temperatures has two important consequences:

(1) The geometrical relationship between the cluster volume and the cluster surface area (surface area $\propto n^{(d-1)/d}$ where d is the dimesionality) depends on the cluster compactness, and since the heart of the clusters are usually compact, on the cluster size. In other words, this geometrical relationship is satisfied at a much smaller cluster size at lower temperatures. For example, for $T=0.9T_c$, n has to be ≥ 90 for this relation to be valid, whereas at $0.4T_c$ it

is valid for $n \geq 10$.

(2) The second more important consequence of geometry is its effect on cluster reactivity. Clusters with straight edges and sharp corners (i.e. square or rectangular clusters) are virtually inactive, until they gain an atom from some other cluster or, less commonly, lose an atom to the matrix, at which time they become "hyperactive", and they diffuse, dissolve, or change shape very dynamically until they again reach an inactive configuration. (This aspect was seen very well in the computer generated movies). At very low temperatures, all the clusters become inactive, whether rectangular or not. The resulting low reactivity at low temperatures results in the prolongation of stage 3 of the reaction. As the temperature is increased, i.e. as the clusters become more and more diffuse, and the matrix concentration of solute increases, stage 3 becomes shorter, and finally disappears.

(ii) Relative jump probabilities:

The basic step in the coarsening reaction in our model is bond interchange. There are several types of bonds (seven types for the square lattice) with different values of interchange energy ΔE associated with their interchange (see Table I). The coarsening reaction is controlled by the probabilities of each of these types of bonds (this depends on the temperature and ΔE) and on their relative populations. Figure 16 shows the actual number of bonds that interchange with energy change ΔE per interchange. Whereas low energy jumps are not very sensitive to temperature, high energy jumps are "extremely" sensitive. It is seen from the figure that 94% of the jumps are of $\Delta E=0$ at $0.3T_c$ compared to 53% at $T=0.8T_c$. Comparatively, the population of the bonds of these types are 15% and 20% of the total bonds. The zero energy jumps correspond to either single atom movement on the cluster or single atom diffusion. For the case of $0.3T_c$, it is 97% single atom movement of the cluster dur-

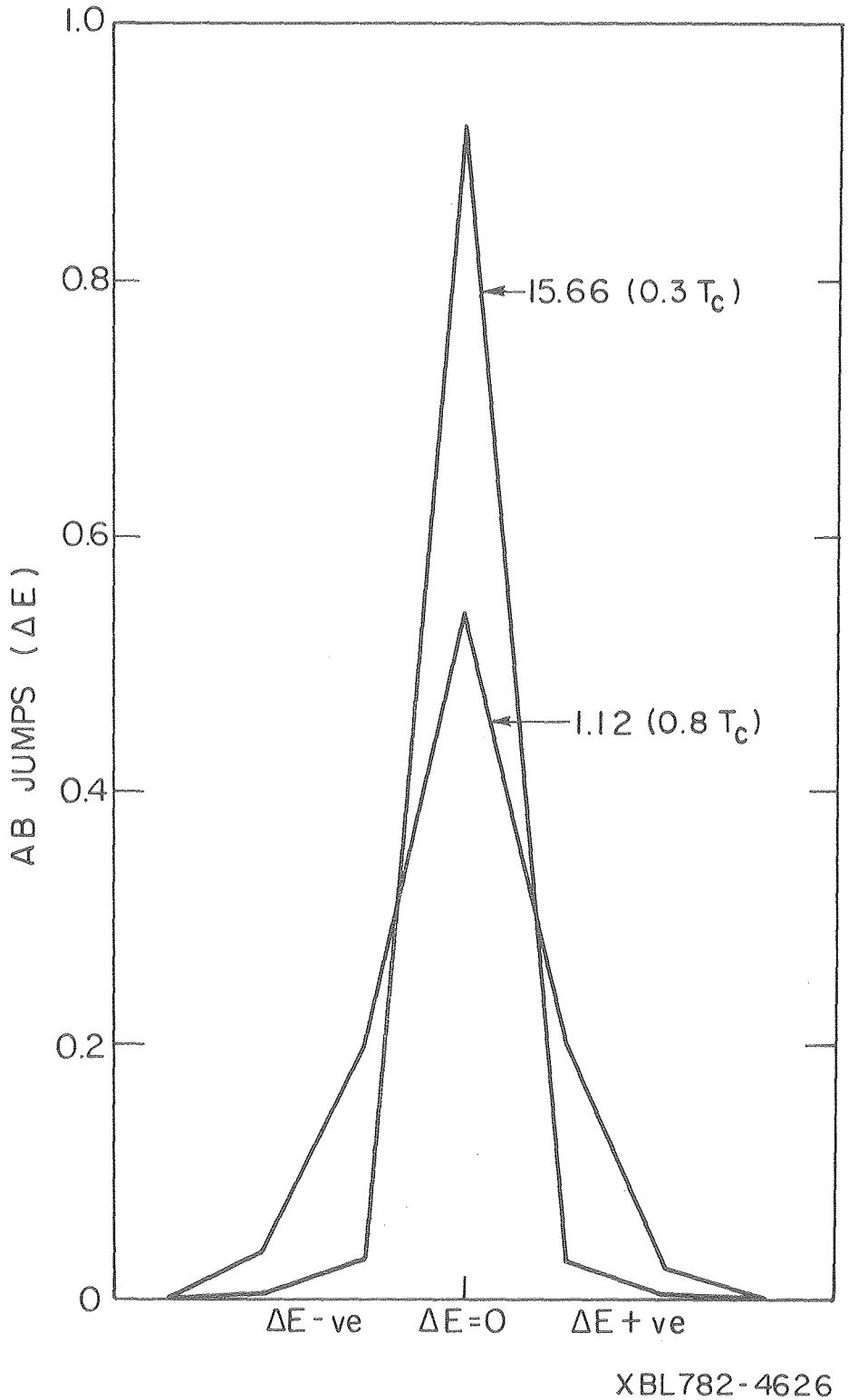

Fig.16. Plots showing the fractional number of AB jumps of different types vs the energy change involved in these jumps at $0.3T_c$ and $0.8T_c$. The numbers by the plots indicate the ratio of AB jumps of $\Delta E=0$ to AB jumps of $\Delta E\neq 0$.

ing stage 3 leading to some extent of cluster spherodization. Cluster diffusion, which usually involves high energy jumps, is lessened in this stage due to many clusters becoming inactive. The small diffusivity that still exists is responsible for the small extent of coarsening in this stage.

(iii) Matrix concentration of solute:

The solubility of the precipitate plays an important role in the coarsening reaction. For the Ising model the equilibrium concentration of solute atoms in the matrix keeps decreasing for T below T_c, and is nearly zero below about $0.4T_c$ for the square lattice. Both the LS and Binder mechanisms work on the presumption of soluble precipitates. If the precipitates are nearly insoluble, atoms cannot leave the precipitate, and coarsening by the LS mechanism is extremely slow. Due to the compact geometry of the precipitates associated with low solubility, Binder's mechanism also becomes inoperative. Thus at very low temperatures we

don't expect to see any significant amount of coarsening after the initial stages.

At somewhat higher temperatures, Binder's mechanism becomes operative at small cluster sizes, but clusters of larger size become inactive i.e. Binder's mechanism decays. Due to the compact geometry of clusters and the low solubility, we have a situation where dissolution of atoms from the precipitate to the matrix is a difficult step. This leads to a "solubility controlled" coarsening. However, not all the clusters are completely inactive. Even clusters that are nearly square have or develop active centres such as kinks and double kinks which enable them to be more active in those regions. This leads at late times to a combination of "solubility controlled" (SC) and LS coarsening to occur.

(b) Effect of temperature on reaction rate: The role played by the geometry can be understood by separating it from (ii) and (iii). We can calculate the jump probabilities for each temperature and also the relative population

of bonds, from which the expected reaction rate can be calculated. It is expected that the reaction rate will be different than the calculated rate: (1) at early times, because the initial bond populations are those typical of $T=\infty$ and it takes time to reach those typical of the experimental temperature; (2) at low temperatures, because geometrical restraints prevent or delay the reaching of steady state relative bond populations.

The reaction rate can be measured in terms of t^*, the time required for an AB exchange, which depends on the population of AB bonds and on the relative probability of an AB type jump vs an AA or BB type jump. The number of AB exchanges per unit time given by $1/t^*$ would be a good measure of the system reactivity R^*, since only such exchanges change the energy or microstructure of the system.

Based on the assumption that the bonds have reached constant asymptotic relative populations (typical of each temperature) in accordance with the energies associated with

them, we can calculate the expected time per AB bond jump as

$$t^* = \left[\frac{N_{AB}}{N_{total}} \sum_i N_i P_i \right]^{-1} \qquad V.1$$

where P_i are the jump probabilities of the types i=1,7 and N_{AB} is the total number of AB bonds, N_{total} is the total number of bonds in the system and N_i is the partition factor which gives the fraction of the N_{AB} bonds in the various types. This formula predicts that at infinite temperature, $t^*=1/f$ where f is the fraction of bonds of the AB type, $f=c(1-c)$, c being the impurity concentration. At any lower temperature, t^* is greater than this value. [If we had a highly supersaturated solution, we can have $t^*<<1/f$ as happens at the beginning of the reaction. As time increases, t^* reaches values typical of each temperature]. At infinite temperature N_i is independent of the energy associated with each bond type, and depends oly on the multiplicity of the bond type (which in turn depends on the impurity concentration ad the lattice geometry). The calculations of N_i at infinite temperature and their values for a concentration of

0.2 are given in Table I. At any other temperature, the values of N_i are modified by a factor $\propto \exp(\Delta E/kT)$.

Figure 17 shows the plots of t* vs T after 1×10^6 and 5×10^6 exchanges. The prediction given by equation (1) is also given. The expected deviations of the simulation results from the calculated values are observed in the figure. The deviations at lower temperatures can be explained by reference to Figure 16. Although N_{AB}/N_{total} keeps decreasing with temperature and the partition among the seven types of these N_{AB} bonds does tend to favor the lower energy types as we lower the temperature, at very low temperatures the system finds itself in a high energy position ($N_{AB}/N_{total} >>\!\!\propto_{\infty}$) which favors $\Delta E=0$ bonds profusely. This means that the jump keeps occuring at higher frequencies, but N_{AB} does not decrease. Thus the system is frozen in a local state of neutral equilibrium of high energy and high reactivity, escape from which is difficult because of geometric restraints. When it does escape and move towards

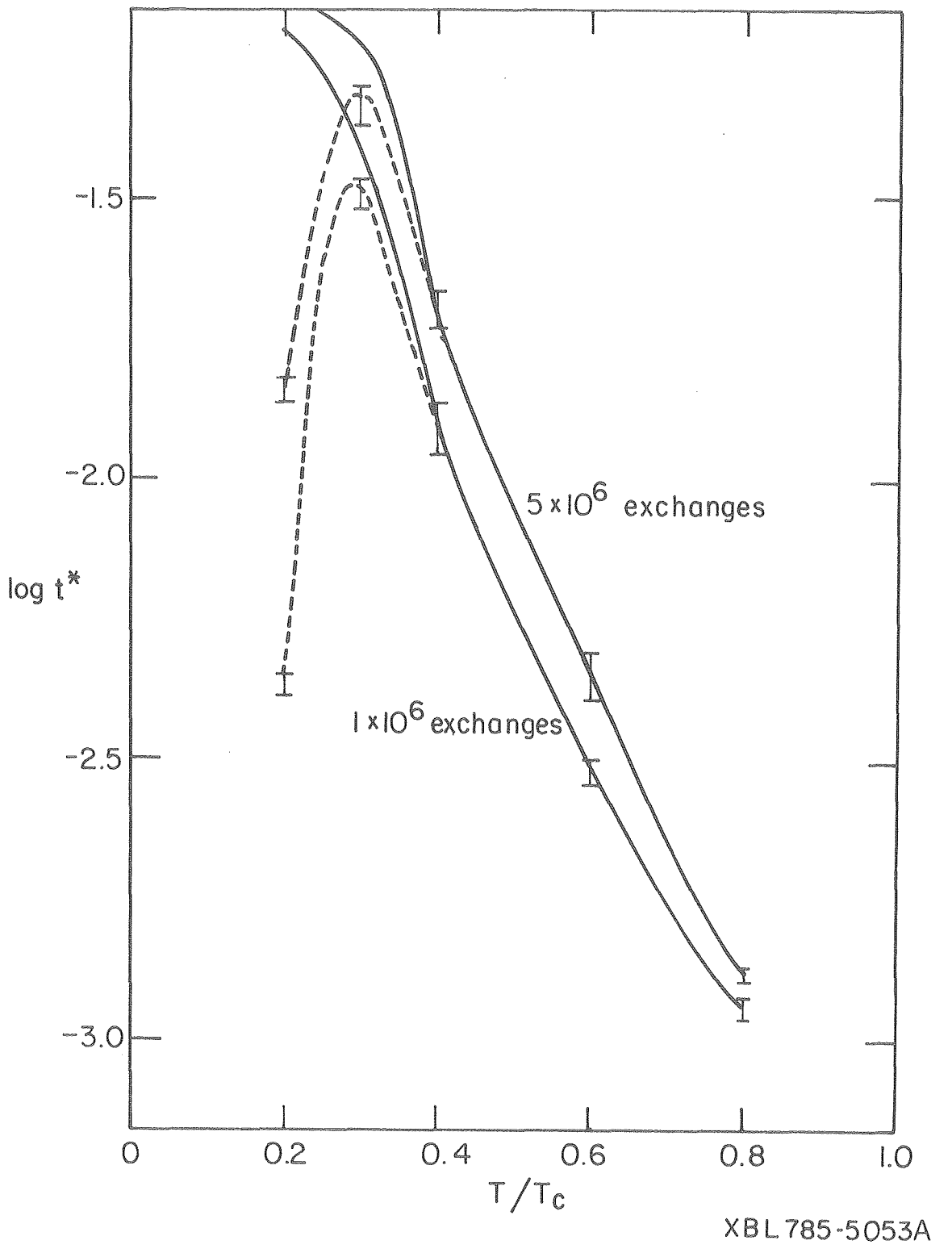

Fig. 17. The average time between successive AB jumps (t*) vs temperature after 1×10^6 and 5×10^6 AB jumps. The data bars are simulation data, the continuous curves are obtained from asymptotic bond populations, and the dotted curves indicate the deviation.

the equilibrium state, the t* should follow the calculated curve.

When the system is quenched from infinite temperature to the reaction temperature it tries to (1) equilibrate the composition; (2) equilibrate the relative bond populations (surface profile); and (3) "minimize" energy. Equilibrium of composition is achieved at very short times at all temperatures. Equilibrium of relative bond populations is achieved at short times at higher temperatures but takes longer at lower temperatures. There is thus a competition between (2) and (3) at lower temperatures.

The reactivity R* of the system (=1/t*) keeps decreasing with time. When the system enters the equilibrium state (which is dynamic) the reactivity reaches a constant value. By starting out with the equilibrium state at T=0 (lowest energy state) and equilibrating at the reaction temperature, this final reactivity can be found. The reactivity at any time during coarsening at that temperature starting from the

random initial configuration is them given approximately by $\frac{\epsilon}{\epsilon_\infty} \times R_\infty$. On Figure 18 the energy values (starting from the energy for random distribution) and the corresponding t* values obtained from simulation are shown as data bars. The continuous curves are the t* values calculated from $t^* = 1/R^* = \epsilon_\infty / (\epsilon \times R_\infty)$. That is, the continuous curves indicate the t* values when the partition of bonds into types reaches a steady value, corresponding to the distribution in the equilibrium state. The point where the data bars reach the continuous curve signifies the time when the bond populations have reached a steady state, since the same distribution of bonds into types can be expected to be maintained through to the equilibrium state. When steady state bond populations are reached, the system is now only trying to reach "minimum energy" state, and this signifies the end of stage 3.

Figure 14 shows the relative bond populations for $0.4T_c$ for a concentration of 0.2. The equilibrium values are also

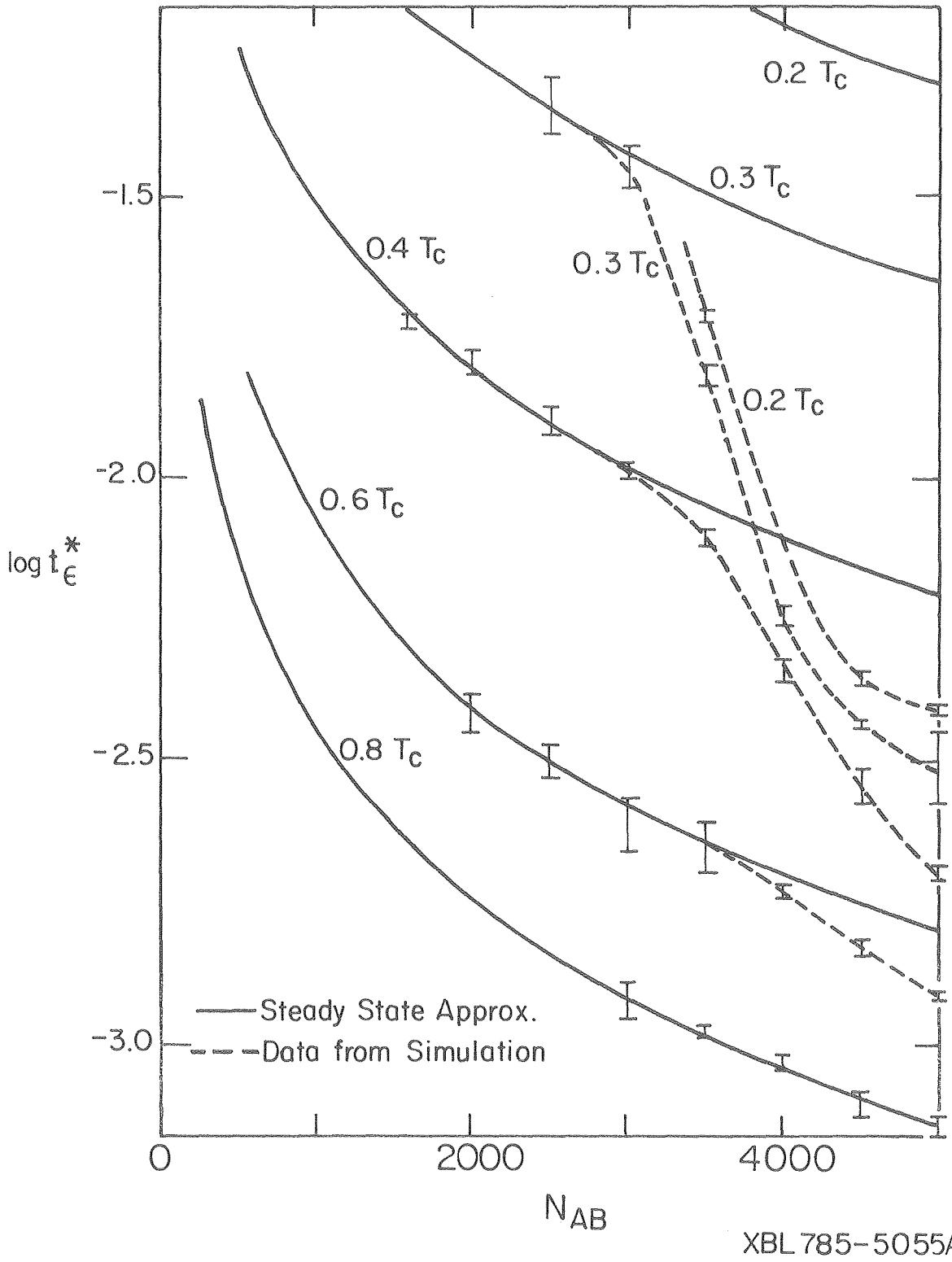

Fig. 18. The average time between successive AB jumps (t*) vs the number of AB bonds in the lattice (N_{AB}). The data bars are simulation data, the continuous curves are obtained from asymptotic bond populations, and the dotted curves indicate the deviations.

indicated on the plot. It is clearly seen that the relative bond populations (F_i) asymptote to the equilibrium values. More significant than F_i are F_iP_i values which actually determine the probability of jump of the various types, as also ΣF_iP_i which determines the overall jump probability. Figure 19 and figure 20 show the values of F_iP_i vs. time for a 20%B atom alloy at $0.8T_c$ and $0.4T_c$. The equilibrium values are also indicated. We can see that the equilibrium values of F_iP_i satisfy the relation:

$$F_iP_i = F_{(8-i)}P_{(8-i)} \qquad \text{V.2}$$

This is understandable because bonds of type i yield bonds of type (8-i) upon interchange, and at equilibrium these rates of interchange must be equal. During the kinetic evolution if we take the time average over long periods of time, the relationship

$$\sum_{i=1}^{i=3} F_iP_i \geq \sum_{i=5}^{i=7} F_iP_i \qquad \text{V.3}$$

is satisfied, which yields the eventual decrease in energy. This inequality gradually diminishes and as equilibrium is

$T=0.8T_c$

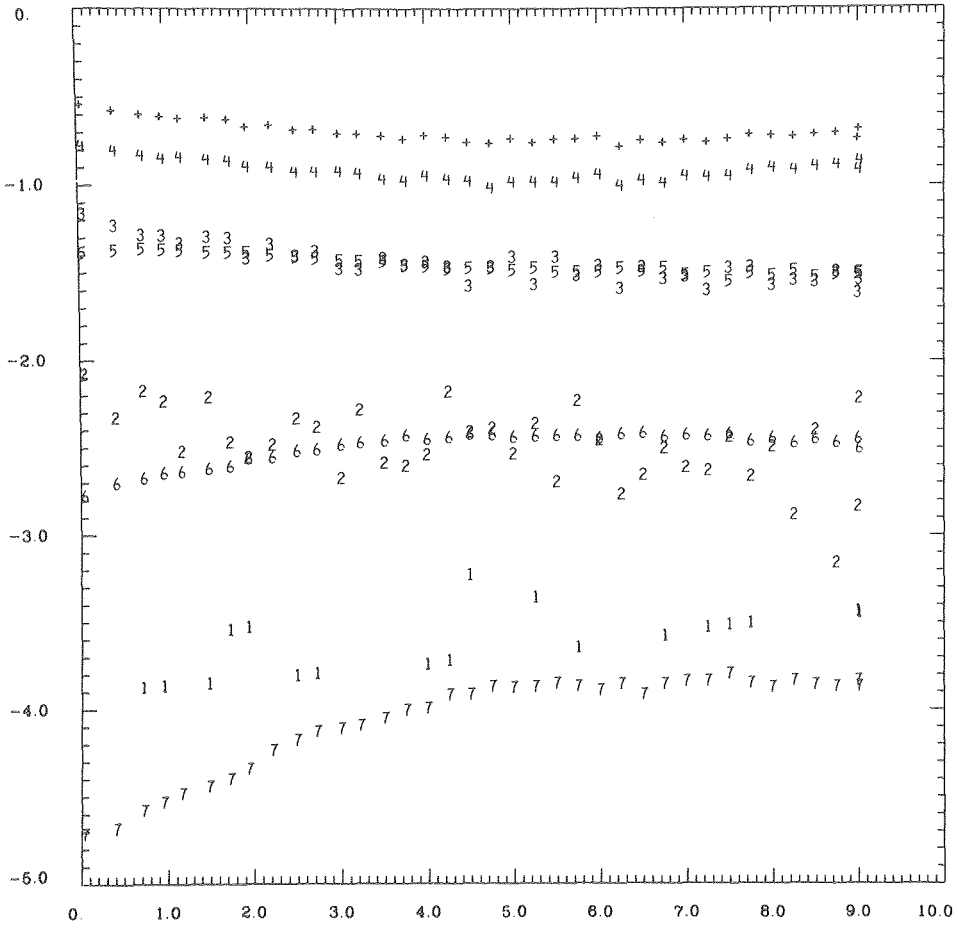

XBL 798-11040

Fig.19. Plot of F_iP_i vs. time for a 20% B alloy at).8 T_c.

$T=0.4T_c$

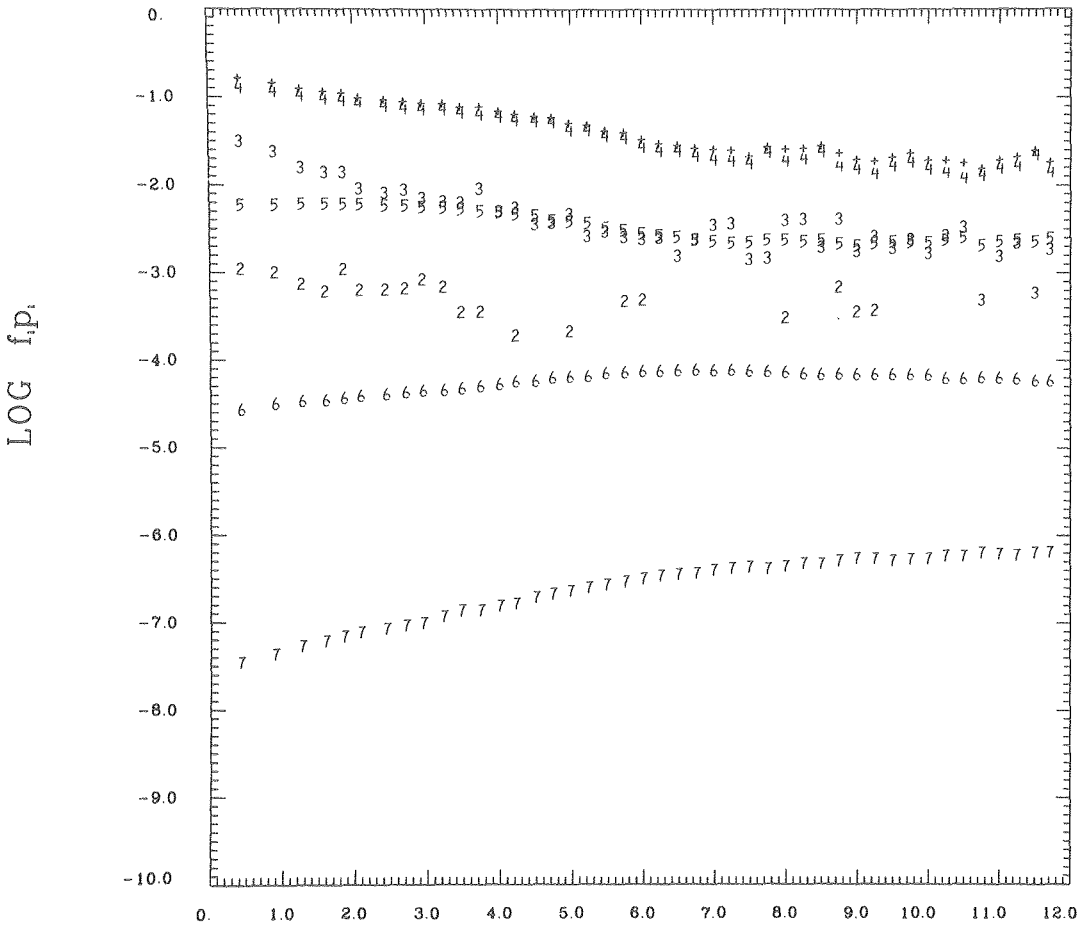

XBL 798-11039

Fig.20. Plot of $F_i P_i$ vs. time for a 20% B alloy at $0.4T_c$.

approached, the two sides of equation V.3 become equal.

Figure 21 shows the values of $\Sigma F_i P_i$ for various temperatures for an alloy of 20%B atoms. The equilibrium values are also indicated. $\Sigma F_i P_i$ decreases continually with time, asymptoting to the equilibrium value. That is the reactivity of the system keeps on decreasing until it reaches that of the equilibrium state. It is observed in Figure 18 that the asymptotic value of $\Sigma F_i P_i$ is in fact lower than the equilibrium value for $0.8T_c$ as also for $0.6T_c$. If we go back to Figure 10 we see that the asymptotic values of $F_i P_i$ for $0.8T_c$ all are close to the equilibrium values, except for i=4 (zero energy exchange), which is lower than the equilibrium value. This effect is thus the caused by an underpopulation of bonds of type 4. This can be understood if we consider the population of A atoms in B clusters. At equilibrium, when there is a single big B cluster, you do have A atoms inside the B cluster which contribute to type 4 bonds (each A atom floating in a B cluster

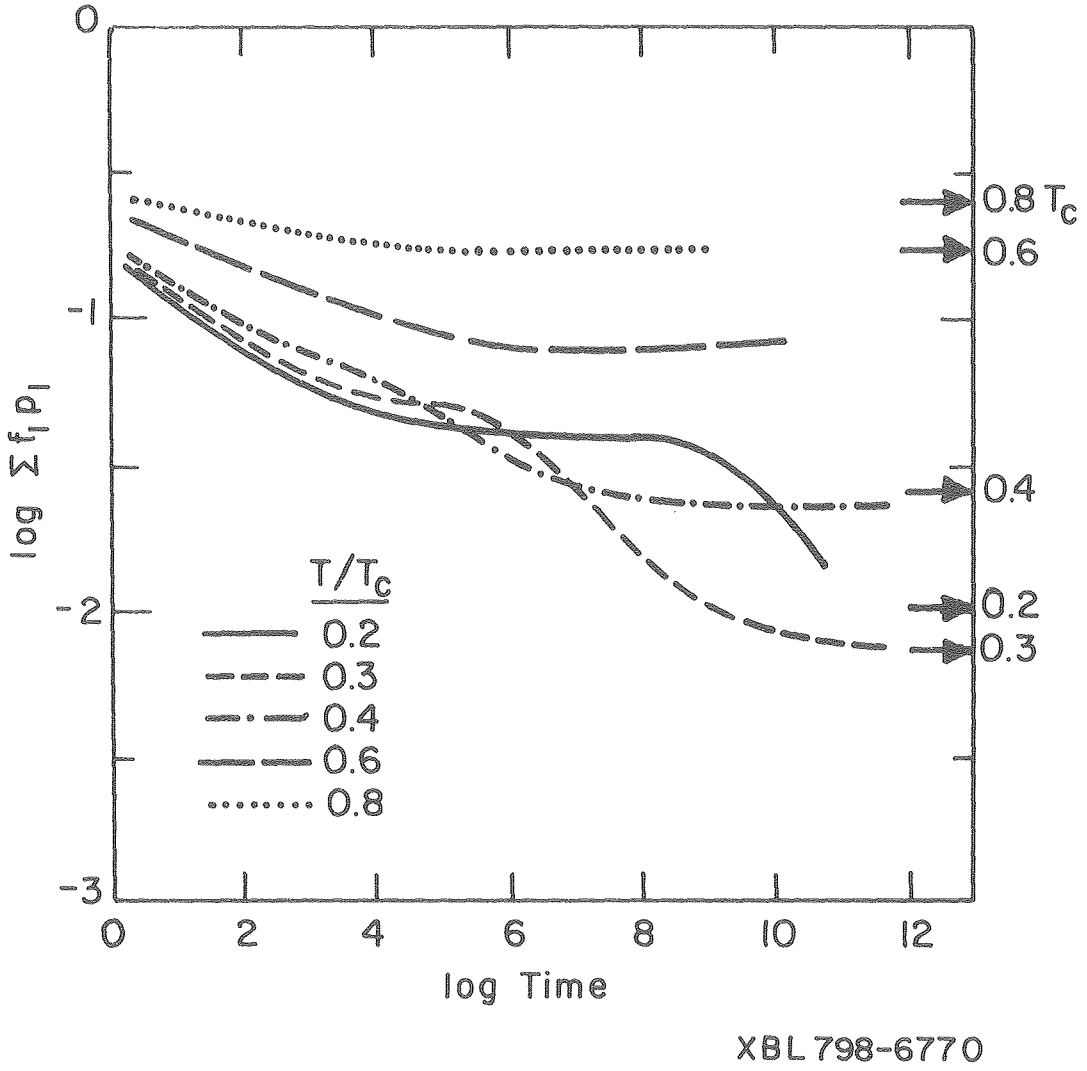

Fig.21. Plot of $\Sigma F_i P_i$ vs. time for a 20% B alloy at different temperatures.

gives four type 4 bonds). Whereas when the cluster sizes are smaller, as happens to be the case at earlier times, the A atoms are present in lesser concentrations in the B clusters, and thus the relative concentration of type 4 bonds is lower than at equilibrium. important at lower temperatures because the equilibrium concentration of A atoms in B clusters is itself small.

3. Effect of Composition

The general coarsening behaviour remains largely unchanged after changes in composition. However, composition has these four effects: (a) Higher composition means a bigger difference between the infinite temperature state and the experimental temperature state, and hence increases the initial relaxation period. (b) The cluster diffusion mechanism seems to be more predominant at higher compositions. (c) Table VII shows the slopes of $\langle n \rangle = t^a$ for 10% B and 20% B case at roughly the same time range. In the case of 10% B, a higher fraction of B atoms are in the matrix,

aiding the freer flow of atoms between the particles, as also their diffusion. Thus the slopes are somewhat higher for the 10% case than for the 20% case. It is tempting to conclude that the reason for this could be because with 10% B the LS assumption of widely dispersed precipitates is better satisfied. However, Ardell's analysis[5] argues that the time exponent does not depend on the volume fraction of the precipitate. (d) Steady state bond populations are reached much faster at lower concentrations.

4. Effect of Lattice Type

One other lattice type, the hexagonal lattice, was simulated. The phase diagram for the two dimensional hexagonal lattice and the two dimensional square lattice are roughly the same (very close to each other) in the nearest neighbor case. Hence there would not be much difference in equilibrium properties determined by the phase diagram. However it is geometrically different from the square lattice: the nearest neighbors of a hexagonal lattice are

nearest neighbors of each other, which is not the case with square lattice. This will affect the kinetics to some extent. (This fact also makes the number of bond types only 7 instead of 13 although there are 6 nearest neighbors for each atom).

The hexagonal lattice also shows the same four stage behaviour as the square lattice. Figure 10 shows an example of the <n> vs time curve for a hexagonal lattice. Some interesting differences between the square and hexagonal lattices are:

(1) Very soon in the simulation, the B atoms form into many small clusters, whereas it takes more time for this to happen in the square lattice. This is to be expected since hexagonal lattice has more nearest neighbors.

(2) The bond type frequency peak moves to type 7 after as few as 2000 jumps. This does not happen in the case of the square lattice even after 10^6 jumps for many cases.

(3) The geometry of the hexagonal lattice provides the possibility of cluster diffusion by zero energy jumps. For example a 2 atom cluster can diffuse without any high energy jumps here which is impossible in a square lattice. This factor has these effects:

(a) Binder's mechanism is more predominant at early times, the slopes corresponding much more closely to the predicted ones.

(b) The smallest cluster unit during the frozen period at very low temperatures becomes 3 instead of 2 atoms.

(C) Cluster spherodization can be observed more clearly in the hexagonal lattice. The slopes in stage 3 in general are higher than for the square lattice.

(4) The effects of temperature and composition have not been studied in detail for the hexagonal lattice, but

the trend seems to be similar to that of the square lattice.

CONCLUSIONS

(1) Both excess energy $\langle \epsilon - \epsilon_\infty \rangle$ and the average cluster size $\langle n \rangle$ are found to obey simple power law relationships with time, $\langle \epsilon - \epsilon_\infty \rangle = t^{-b}$, $\langle n \rangle = t^{a}$, the exponents corresponding to LS mechanism at very late times.

(2) The general case of precipitation and coarsening in binary Ising square lattice follows four stages:

(i) initial relaxation

(ii) Binder's mechanism (cluster coagulation)

(iii) transition stage — cluster coagulation declines

(iv) LS and SC mechanisms set in, Ostwald ripening by diffusional processes.

(3) Temperature affects the general four stage mechanism in

such a way that at very high or very low temperatures only three stages are seen. At high temperatures stage (iii) is almost absent and stages (ii) and (iv) overlap very much; as the temperature is lowered, stage (iii) becomes longer, and at very low temperatures stage (iv) is not reached in reasonable experimental time.

(4) Temperature also affects cluster geometry, the clusters being more compact and faceted at lower temperatures.

(5) Low temperature simulations, where solubility is low never reach significant coarsening rates, although the dimensionless diffusivity is the same as that at high temperatures. This suggests that clusters with very low solubility can resist coarsening.

(6) Temperature is also seen to affect the time taken to reach the constant asymptotic bond-type populations. This explains the unusual behaviour of t* (average time between successive AB interchanges) with temperature.

(7) Although composition does not affect the general coarsening behaviour, a higher composition makes the particle growth kinetics a little sluggish. Also, the cluster diffusion and coagulation mechanism is seen to be more predominant at higher compositions.

(8) The coarsening kinetics on a hexagonal lattice are very similar to those on a square lattice.

ACKNOWLEDGEMENTS

This work was supported by the Division of Materials Sciences, Office of Basic Energy Sciences, U.S. Department of Energy.

REFERENCES

1. C. Wagner, Electrochemie, 65, 243 (1961).

2. Lifshitz and Slozov, J. Phys. Chem. Solids, 19, 35 (1961).

3. M. Kahlweit, Colloid Interface Sci., 5, 1 (1975).

4. C. A. Johnson, Surface Science, 3, 429 (1964).

5. A. J. Ardell, Acta Met., 20, 61 (1972).

6. K. Binder, Phy. Rev. B, V15, 9, 4425 (1977).

7. L. D. Fosdick, Methods in Computational Physics, (B. Alder et al. eds. Academic Press, New York, 1963), V. 1.

8. K. Binder et. al. in Nucleation Vol. III, ed. Zettlemoyer (preprint).

9. Lebowitz, Phani and Tsai, AIME Winter Meeting, Feb 26-March 1, 1978, Denver, Colorado.

10. N. Metropolis, J. Chem. Phys. 21, 1087 (1953).

11. G. W. Guggenheim and P. H. B. Meijer, J. Comp. Phys., 20, 50 (1976).

12. K. Binder and D. Stauffer, Adv. Phys. (1976).

13. O. Penrose and J. L. Lebowitz, in Nucleation Vol. III, ed. Zettlemoyer (preprint).

14. K. Binder and D. Stauffer, Phy. Rev. Lett., 33, 1006 (1974).

15. G. W. Greenwood, The Mechanism of Phase Transformations in Crystalline Solids, Inst. of Metals Monograph #33, 103 (1969).

FIGURE CAPTIONS

Fig.1. Phase diagram of the binary Ising square lattice, indicating the points of simulation reported here. The dotted line shows the limit of metastability, assuming a free energy density of the form $f(C_{cr}) = A(C-C_{cr})^2+B(C-C_{cr})^4+f(C_{cr})$ where C_{cr} is the concentration at the phase boundary.
XBL 789-5834

Fig.2. A possible representation in the computer (b) of the (100) plane of an FCC system.
XBL 795-6201

Fig.3. Topological transformation of the two dimensional hexagonal lattice into an equivalent square lattice.
xbl 794-6144

Fig.4. Transformation of a square lattice into a topologically equivalent one dimensional lattice.
xbl 794-6145

Fig.5. Transformation of an FCC lattice into a topologically equivalent simple cubic lattice.
xbl 794-6143

Fig.6. Flow chart of the computer code.
xbl 794-9352

Fig.7. Equilibrium structure of a 114*114, 20% square lattice at different temperatures.
.sp

Fig.8. Plots of average cluster size <n> vs. time for a 20% B alloy at various temperatures. Note that the same dimensionless diffusivity is used for all the temperatures.
XBL 782-4575

Fig.9. Plots of excess energy $\langle \epsilon - \epsilon_\infty \rangle$ vs. time for a 20% B alloy at various temperatures.
XBL 798-6791

Fig. 10. Plots of average cluster size <n> vs. time for a 80*80 hexagonal lattice of 20% B concentration.
XBL 7811-6133

Fig. 11. Time evolution of a 120*120 square lattice of 20% B concentration at $0.8T_c$. (a) Initial random configuration; (b) configuration after 89 time units and (c) configuration after 1341 time units.
XBL 7810-12103

Fig. 12. Snapshots during the time evolution of a 120*120 square lattice of 20% B concentration at $0.3\ T_c$ showing cluster diffusion and coagulation mechanism for example, in regions marked with big circles. Notice, also, the atom by atom transfer mechanism, such as in the area marked with the small circles.
XBL 7810-12100

Fig. 13. Plot of average cluster size <n> vs. time for a 120*120 square lattice of 20% B concentration at a reduced temperature of 0.4T. Also shown is the corresponding values of relative bond population of bonds of type 4 (see Table I).
XBL 7811-6093

Fig. 14. Plots of jump type fractions vs. time for a 20% B alloy at $0.4\ T_c$.
XBL 798-11038

Fig. 15 Microstructure of a 20% B alloy at roughly the same time after quench to (a) $0.4\ T_c$ and (b) $0.8\ T_c$.
XBL 7810-12012

Fig. 16. Plots showing the fractional number of AB jumps of different types vs. the energy change involved in these jumps at $0.3\ T_c$ and $0.8\ T_c$. The numbers by the plots indicate the ratio of AB jumps of $\Delta E=0$ to AB jumps of $\Delta E\neq 0$.
XBL 785-5053

Fig. 17. The average time between successive AB jumps (t*) vs. temperature after 1×10^6 and 5×10^6 AB jumps. The data bars are simulation data, the continuous curves are obtained from asymptotic bond populations and the dotted curves indicate the deviation.
XBL 785-5053

Fig. 18. The average time between successive AB jumps (t*) vs. the number of AB bonds in the lattice (N_{AB}). The data bars are simulation data, the continuous curves are obtained from asymptotic bond populations and the dotted curves indicate the deviations.
XBL 785-5055

Fig. 19. Plot of $F_i P_i$ vs. time for a 20% B alloy at 0.8 T$_c$.
XBL 798-11040

Fig. 20. Plot of $F_i P_i$ vs. time for a 20% B alloy at 0.4T$_c$.
XBL 798-11039

Fig. 21. Plot of $\Sigma F_i P_i$ vs. time for a 20% B alloy at different temperatures.
XBL 798-6770